Numerical Modelling of van der Waals Fluids

Tinuade Odeyemi

A thesis submitted to the

Faculty of Graduate and Postdoctoral Studies

In partial fulfillment of the requirements

For the MASc degree in Environmental Engineering

Ottawa-Carleton Institute for Environmental Engineering

University of Ottawa

Abstract

Many problems in fluid mechanics and material sciences deal with liquid-vapour flows. In these flows, the ideal gas assumption is not accurate and the van der Waals equation of state is usually used. This equation of state is non-convex and causes the solution domain to have two hyperbolic regions separated by an elliptic region. Therefore, the governing equations of these flows have a mixed elliptic-hyperbolic nature.

Numerical oscillations usually appear with standard finite-difference space discretization schemes, and they persist when the order of accuracy of the semi-discrete scheme is increased. In this study, we propose to use a Chebyshev pseudospectral method for solving the governing equations. A comparison of the results of this method with very high-order (up to tenth-order accurate) finite difference schemes is presented, which shows that the proposed method leads to a lower level of numerical oscillations than other high-order finite difference schemes, and also does not exhibit fast-traveling packages of short waves which are usually observed in high-order finite difference methods. The proposed method can thus successfully capture various complex regimes of waves and phase transitions in both elliptic and hyperbolic regimes.

Acknowledgements

I would like to thank my supervisors, Dr. Majid Mohammadian and Dr. Ousmane Seidou, for their unrelenting effort, support, and guidance throughout my degree, for setting me right in all the times I went wrong, and for being patient with me.

A huge thank you goes out to my family—my parents and siblings—for praying along with me throughout this journey. To my fiancé, I thank you for believing in me and pushing me with encouraging words even when I almost gave up.

And to the Almighty, ever-faithful God, whom I leaned on throughout my program and who never let me down, I say the biggest thank you.

Contents

Table of Figures

List of Tables

List of Abbreviations

DNS	Direct Numerical Simulation
FFT	Fast Fourier Transform
GCL	Gauss-Chebyshev Lobatto
ODE	Ordinary Differential Equation
PDE	Partial Differential Equation
NS	Navier- Stokes

List of Symbols

a	measure of intermolecular attraction
A	m × m matrix
b	average volume removed by a mole of particle
D_N	Chebyshev spectral differential method
e_j	eigenvectors
E	Energy
fx, fy, fz	flux vectors in x, y, z directions
K	Boltzmann's constant
L	Wave length
m	vector of variables
n	number of moles
P	Pressure
Q	vector of m components
R	universal gas constant
T	absolute temperature
U	velocity of fluid

V	volume of vessel
α	dispersion coefficient
ε	viscosity coefficient
τ	specific volume
ρ	density
ω	wave number

Chapter 1: Introduction

Recently, interest in computer simulations of interfacial dynamics for liquid–vapour coexistence has greatly increased. Liquid-vapour flows are observed in many everyday situations. The formation of a cloud, boiling water in a pot, or the rise of bubbles in gaseous drinks are fascinating everyday examples where liquid–vapour coexist in nontrivial flow situations.

When temperature and pressure are respectively lower and high than certain values (which depend on gas type), van der Waals forces become important and should be considered in the equations of motion. Such cases are observed in some applications such as certain industrial refrigerators. Simulating and understanding the dynamics of this phenomenon is also very important in some situations, such as the prediction and control of nuclear accidents in refrigerated nuclear reactors.

The governing equations for gas and fluid flow are Navier-Stokes (NS) or Euler equations. In these equations, the pressure is specified by the equation of state. In most practical cases, the ideal gas assumption is valid and the corresponding equation of state is used as explained in Chapter 2. However, when intermolecular forces become important, the ideal gas equation of state is not valid. The inclusion of the intermolecular forces in the equation of state leads to the van der Waals equation of state. The NS system with van der Waals equation of state (NSW) is a complex system, and numerical models cannot resolve all processes in the fluid.

The complexity of the NSW system is due to the special form of the van der Waals equation of state. This equation of state is not convex as explained in Chapter 2. Indeed, the van der Waals

equation of state in general has a convex-concave form. This form leads to a complex behaviour of NSW system; namely a hyperbolic-elliptic behaviour, which is explained in chapter 3.

The solution of NS system with van der Waals equation of state is also important for developing turbulence models (parameterization schemes). In many conventional engineering computational fluid mechanics approaches, effective hydrodynamic equations are used in which the presence of bubbles or drops is modelled by the introduction of void or vapour fraction. Coarse-grained approaches need empirical constitutive equations that are not always available, and moreover, the detailed interface dynamics of bubbles and droplets is not obtained in these methods.

Therefore, in order to obtain precise information about large-scale motions, small-scale processes should be modelled via closures (turbulence modeling). An important part of the research in liquid–vapour fluid mechanics deals with the determination of these closure laws. One way to develop such closures is the employment of very high-resolution models that can capture small-scale features of phase transition. Indeed, one of the important ingredients in liquid–vapour flows is the knowledge of the transfers that occur at the interfaces. Therefore it is essential to model these transfers and to be able to model the interfaces.

In particular, liquid-vapour flows which are specified by the van der Waals equation of state are an important class of problems in fluid mechanics and material sciences, and are governed by a nonlinear system of elliptic-hyperbolic equations, as explained in Chapter 3. The main characteristic of hyperbolic systems is that they typically include shock waves in the solution which basically represent a sudden change in the numerical solution. Such sudden changes are typically observed within a few computational grid points in the results. Further characteristics of the elliptic-hyperbolic systems will be discussed in chapter 3.

Pioneering mathematical studies on van der waals flows were conducted by Slemrod et al. (1981), who investigated self-similar approximations to the Riemann problem. The Riemnn problem is defined by a discontinuity in variables as explained in Chapter 3. As mentioned before, nonlinear hyperbolic equations may generate discontinuous solutions called shock waves, which can be classical or non-classical. Classical (compressive) shock waves satisfy standard entropy criteria (see e.g., LeFloch, 2001), which basically state that the mathematical entropy cannot decrease across the shock. However, non-classical (under-compressive) shock waves, also called subsonic phase boundaries in phase transition problems, violate those standard entropy criteria. Therefore, a special condition, the so-called kinetic relation, is needed to uniquely specify the solution. Numerical solution of these shock waves is a challenging issue, and most available numerical methods face problems in simulation of those waves, in particular leading to inaccurate kinetic functions (LeFloch and Mohammadian, 2008). In this project, we consider a class of van der Waals flows with non-convex flux functions. In these flows, non-classical under-compressive shock waves can develop. Such waves, which are characterized by kinetic functions, violate classical entropy conditions.

Several methods are available for numerical solution of partial differential equations which include finite volume methods, finite element schemes, spectral and point vortex methods, and Lagrangian or semi-Lagrangian methods. These schemes are mainly different in the properties of the obtained numerical solutions such as conservation of mass, momentum and energy, the computational grid, computational cost, applicability to problems with complex and moving boundaries, etc. In the following, we will briefly review certain characteristics of these schemes.

High-order upwind finite volume methods are one of the most popular schemes in fluid dynamics, especially in hyperbolic regimes such as shallow water equations, since they

inherently conserve mass and momentum, which is crucial for a correct prediction of shock speed (e.g., LeVeque, 2002). However, despite their considerable success in simulating discontinuities, most upwind schemes lead to a high level of numerical diffusion and energy dissipation in circulating flows (e.g., Mohammadian et al., 2005). Furthermore, most upwind methods encounter problems in the presence of source terms (e.g., Xing & Shu, 2006; Noelle et al., 2007; Mohammadian & Le Roux, 2006), due to an imbalance between the source and flux terms at the discrete level. In the past decade, some techniques, which mostly preserve only steady state conditions, have been proposed to overcome the imbalance problem. However, they are usually expensive and may also encounter problems in unsteady (transient) situations. Mohammadian and Le Floch (2008) performed a series of numerical experiments and found that a combination of the fourth-order Runge-Kutta method for time integration and a tenth-order accurate finite difference scheme in space presents the optimal performance among selected schemes in terms of the compromise between numerical errors and computational cost. In that study, time integration schemes up to the eighth-order Runge-Kutta scheme were also used for time integration, but the gain in numerical accuracy was not justified by the increased computational cost of the higher-order time integration method. This scheme will be used in this project for a comparison with the employed numerical method, and as will be shown, it leads to more numerical oscillations for the present system than the Chebyshev pseudospectral method. Finally, it should be mentioned that slope limiters are commonly used in finite volume methods, and as shown in Mohammadian and Le Roux (2008), they may lead to excessive numerical diffusion of waves. The role of slope limiter is to modify the estimation of gradients such that numerical oscillations are not developed. For example, a class of slope limiters simplifies the

numerical method to a first order upwind scheme, because the first order upwind method leads to oscillation-free results for shock-waves and sharp gradients.

Finite element methods are another family of numerical methods that are usually more expensive than explicit finite volume methods because they typically lead to a system of simultaneous nonlinear equations. However, they can sometimes reach a higher accuracy than finite volume methods by a systematic use of basis functions, especially for smooth problems (e.g., Le Roux et al. 2007 & 2008). The imbalance problem may also arise in finite element methods, particularly when eigenvalue decomposition is performed, such as in discontinuous Galerkin schemes (e.g., Xing & Shu, 2006).

Lagrangian and semi-Lagrangian methods are also widely used in fluid dynamics due to their stability over long time steps. However, they are not the optimal choice for the problems in this project because of the presence of various terms that restrict time-step size due to accuracy considerations rather than stability limitations.

Spectral and point vortex methods are among the most accurate numerical methods and are very popular in turbulence studies due to their low levels of numerical diffusion and oscillation (e.g., Kondaraju et al., 2010; Holmas et al., 2008; Sengupta et al., 2009). Point vortex methods are generally more expensive than spectral methods, but unlike the latter they can be used in complex geometries as well (e.g., Mohammadian & Marshall, 2010).

Spectral methods have been used for a long time in fluid dynamic problems, even before the advent of computers, by using series expansion. Application of numerical spectral and pseudospectral methods in fluid dynamic problems has become popular since the studies of Orszag (1972), Orszag and Patterson (1972), Kreiss and Oliger (1972), and others in the 1970s,

who used spectral methods in direct numerical simulation (DNS) of turbulent flows. For smooth problems over simple geometries, spectral methods can often approach higher accuracies than other numerical methods, and when lower accuracies are required, they need less computer memory than other alternatives because they can typically reach the same accuracy as alternative methods, but with a fewer number of grid points (Trefethen, 2000; Canuto et al., 2006). Indeed, it can be shown that spectral methods have a very fast rate of convergence. For example, the rate of convergence of the Fourier series is exponential for infinitely differentiable functions (Peyret, 2002). In these methods, adding one more grid point is equivalent to adding one more term into the spectral expansion of the variable whose derivative or integral is being approximated. Moreover, some special techniques are available for the calculation of sums, such as Fast Fourier Transform (FFT), which make them attractive choices for numerical solution of PDEs. Fourier spectral methods may encounter problems in non-periodic boundaries caused by the presence of Gibbs oscillations which are certain types of oscillations that are observed close to boundaries due to non-uniform convergence of Fourier series at the boundaries. Therefore, other types of basis functions must be used for non-periodic boundaries, such as Chebyshev or Legendre polynomials (see e.g., Xie & Lin, 2009; Makinde, 2009; Li et al., 2010).

The Chebyshev spectral method uses a polynomial expansion, but over special discrete points, which prevents the oscillatory tendency of polynomials over regularly spaced grid points. This method shares some properties with the Fourier series, such as rate of convergence and the possibility of using a Fast Fourier Transform algorithm, but it does not encounter Gibbs oscillations at the boundaries. Legendre polynomials, which have some interesting mathematical properties, present another alternative; however, a fast summation algorithm is not available for those polynomials. Therefore, the computational cost becomes prohibitive for high-resolution

calculations such as DNS (Peyret, 2002). Chebyshev polynomial expansion is also used in linear stability analysis problems, both in calculation of eigenvalues and in solving problems with constant coefficient; e.g., in semi-implicit algorithms (Canuto et al., 2006).

Finally, pseudospectral methods are a subcategory of spectral schemes, which are widely used for nonlinear partial differential equations. In these methods, calculation of derivatives is performed in the spectral space, while the products are calculated in physical space, which is the space of the values of the unknowns at the discrete points, and the data are efficiently transformed between the two spaces by the FFT algorithm.

The objective of this project is to find suitable methods for van der Waals fluids. To this end, we will evaluate the performance of the Chebyshev pseudospectral methods for van der Waals flows. We will also consider some other commonly used schemes such as the Central-Upwind method, the Ruzanov scheme, the Fourier pseudospectral method, and the Crank-Nicolson scheme. An experimental approach will be employed in which various schemes will be tested and their results will be compared with reference solution. Our main criteria in comparing the performance of various schemes will be the convergence towards the reference limiting solution and the presence of numerical oscillations.

This thesis is organized as follows. In Chapter 2, the van der Waals forces are explained, the difference between ideal and real gases is discussed, and the equations of state corresponding to each case are introduced. In Chapter 3, model equations are briefly reviewed and their derivations are explained. The reason for the mixed mathematical behaviour of the equations (elliptic-hyperbolic) is also briefly reviewed. Chapter 4 presents the numerical approximation of derivatives using the Chebyshev pseudospectral method where several finite difference schemes

up to order 10 are also presented and the details of the Runge-Kutta integration method for temporal integration are given. In Chapter 5, the performance of the model is numerically evaluated for challenging cases such as pure hyperbolic regimes as well as mixed hyperbolic-elliptic interactions, and it is shown that the proposed method performs better than very high-order accurate finite difference schemes of up to order ten, which were recommended in LeFloch and Mohammadian (2008). In Chapter 6, other schemes are compared and the impact of temporal integration accuracy is discussed. Some concluding remarks complete the study.

Chapter 2: Background

To be able to better understand van der Waals Fluids, we need to look into the meaning of equation of state, the ideal gas and the ideal gas equation of state, van der Waals forces, and the van der Waals equation of state.

2.1 Equation of state

In other to properly describe the properties of fluids (gases and liquids), an equation of state is used. An equation of state can be defined as a set of equations that is used to describe the behaviour of matter under a given state and different conditions. It provides a mathematical correlation between the properties of matter at the given state, the most common of these properties being temperature, pressure, and volume. In this chapter, the equations of state that are of importance to us are the ideal gas equation of state and the van der Waals equation of state.

2.2 Ideal gas and Ideal gas law

An ideal gas obeys the ideal gas law. Naturally, most gases behave like ideal gases at standard temperatures and pressures. The ideal gas law which is the equation of state for an ideal gas applies to ideal gases at higher temperatures and lower pressures. The ideal gas equation of state is written as follows:

$$PV = nRT \tag{2-1}$$

where

P = pressure,

V = Volume,

n = number of moles,

T = temperature, and

R = gas constant with its unit depending on the units of P, V, n, and T.

The ideal gas equation of state given above is valid at higher temperatures and lower pressures and it also neglects the size of the molecules. Another important factor that the ideal gas equation of state does not consider is the intermolecular forces. The equation presumes that the forces of attraction between the particles of a gas are not present, and if this is to be true, then we will not have gases condensing into liquids or solids, which is also known as phase transition. This equation of state therefore does not take into consideration phase transitions.

The ideal gas law will not be applicable in circumstances where we have lower temperatures and higher pressures. To be able to accommodate this effect, another equation of state, called the van der Waals equation of state, was developed.

2.3 Real gases

Gases that do not obey the ideal gas equation of state are called real gases. These gases have conditions that do not comply with the ideal gas equation which is applicable for gases at higher temperatures and lower pressures. However, at lower temperatures and higher pressures, gases condense to either liquid or solid, and the ideal gas equation fails. The van der Waals equation, which was created by Johannes van der Waals in 1873, is the equation of state that predicts the behaviour of real gases. As mentioned before, the ideal gas law, in accordance to the kinetic theory of gases, postulates that for an ideal gas:

- Intermolecular forces are not present
- The size of the molecules present is negligible; that is, the molecules are point masses

Van der Waals was able to examine the two points and derive the van der Waals equation for real gases that deviate from the ideal gas equation of state. He modified the ideal gas law in terms of volume and intermolecular forces (i.e., the inter particle interactions between the gas molecules).

In terms of the volume, the ideal gas law only takes into consideration the total volume of the container which holds the gas molecules, which is reasonable at low pressures. However, van der Waals suggested that the volume of individual gas molecules is significant at high pressures. An illustration of this fact can be seen in Figure 2.1.

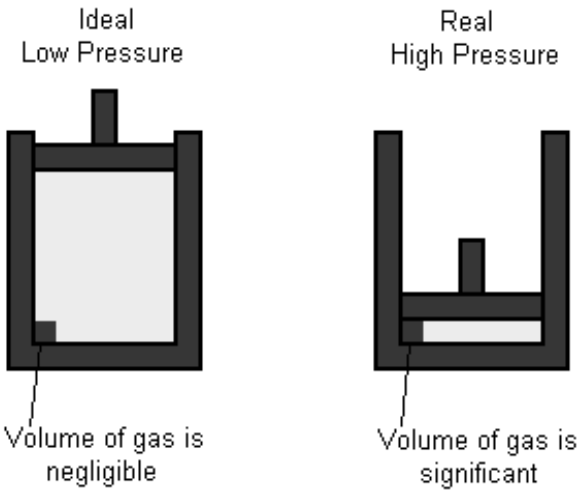

Figure 2.1: Ideal and Real gases

Intermolecular forces in the ideal gas law are neglected or assumed negligible because molecules at higher temperatures have a higher average kinetic energy. Van der Waals, on the other hand, corrected this by stating that at high pressures the intermolecular forces become important, and

the reason is that the distance between the molecules becomes smaller. With these two modifications, the van der Waals equation of state for real gases was developed.

2.4 van der Waals Forces

Chemical bonding in molecules can be achieved either by intramolecular or intermolecular forces. Intramolecular forces can be defined as the forces inside the molecules that keep in place the various atoms that comprise the molecule. These forces are generally stronger, and they make ionic, covalent, and metallic bonds. On the other hand, intermolecular forces are the forces between two or more molecules, and they can be seen in hydrogen bonds. A clear example to differentiate between intra and intermolecular forces is given in the following. A water molecule, which consists of two oxygen atoms and one hydrogen atom, is held together by intramolecular forces (covalent bonds), while the forces that hold together water molecules in ice are intermolecular forces. The intermolecular forces are weaker than the forces acting in the water molecule and are generally easy to break.

These weak intermolecular forces are sometimes called van der Waals forces. These van der Waals forces can be divided into three groups.

1. Forces existing between two dipoles: dipole-dipole forces occur in molecules that are polar or that have a dipole moment (existence of a partial positive and partial negative charge in a molecule). Because of the existence of these positive and negative poles in the molecules, an attraction force exists between them. The positive end of the polar molecule is attracted to the negative end of the adjacent molecule, thereby forming a bond. This is the type of bond seen in two molecules of HCL.

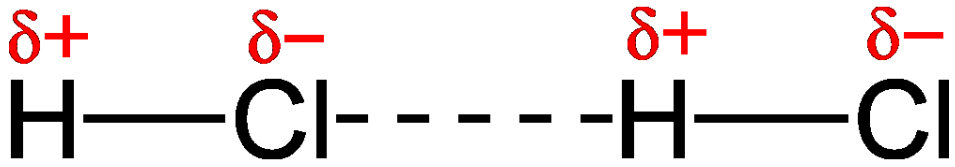

Figure 2.2: Dipole-dipole force of attraction between HCL molecules

2. Forces existing between a dipole and an induced dipole: this type of force occurs when a molecule that has a dipole moment is in contact with another molecule that does not have one. In this case, when the polar molecule comes close to the non-polar molecule, it has the ability to disrupt the uniform distribution of the electrons of the non-polar molecule, thereby creating a brief dipole moment on it which is called an induced dipole. With the non-polar molecule now having a brief dipole moment, a van der Waals force of attraction occurs between the polar and non-polar molecule.

3. Forces existing between two induced dipoles: this involves two molecules that are not polar. The movement of the molecules around each other causes an induced dipole in each molecule, thereby creating an induced dipole - induced dipole force of attraction. Out of all the types of van der Waals forces mentioned above, the induced dipole - induced dipole force is the weakest. This type of force can be seen in two helium molecules.

They can be described as the sum of attractive and repulsive forces between molecules. Van der Waals forces can be weaker, but they play an important role in Polymer Science, Chemistry, and Biology.

2.5 Van der Waals Equation of State

The van der Waals equation of state can be defined as the equation of state for the fluids described above with intermolecular forces and a non-zero volume. The equation is stated as follows:

$$\left(p + \frac{a'}{v^2}\right)(v - b') = kT) \tag{2-2}$$

where

p= gas or liquid pressure,

T= absolute temperature,

k= Boltzmann's constant,

v= volume of the vessel holding the fluid particles divided by the number of particles,

a′= measure of the intermolecular attraction between the particles, and

b′= average volume removed from v by a fluid particle.

The equation above is the simplified form of the van der Waals equation of state. There is a more accepted form of the equation which includes the addition of the Avogadro's constant N_A, the amount of gas molecules n, and the total number of particles nN_A . The van der Waals equation can thus be re-written as

$$\left(p + \frac{an^2}{V^2}\right)(V - nb) = nRT \tag{2-3}$$

where

p= gas or liquid pressure,

V= entire volume of the vessel holding the fluid,

n= number of moles,

a= measure of the intermolecular attraction between the particles= $N^2_A a'$,

b= volume removed by a mole of particle = $N_A b'$,

R= universal gas constant = $N_A k$, and

T= absolute temperature.

The v in equation (2-2) is different from the V in equation (2-3), and they are related in the equation below.

$$v = \frac{V}{nN_A} \tag{2-4}$$

where

V = entire volume of the vessel holding the fluid, and

nN_A = total number of gas/liquid particle.

The equation (2-3) is a correction of the ideal gas law found by van der Waals to account for intermolecular forces between the molecules and the volume of particles. This was achieved as follows:

1. Van der Waals found that the measured volume of the fluid molecules were higher than the ideal or absolute volumes of the fluid molecules, and corrected it as:

$$V_{meas} = V_{ideal} + nb \tag{2-5}$$

Or $V_{ideal} = V_{meas} - nb$ (2-6)

2. In terms of the intermolecular attractions, van der Waals corrected the pressure term in the ideal gas law by stating that direct collision exists between the molecules as they are now considered to have mass (real gas), and with each molecule, there is a negative and positive pole. This allows the positive pole of one molecule to attract the negative pole of another molecule. Therefore, the measured pressure will be reduced:

$$P_{meas} = P_{ideal} - \frac{n^2 a}{V^2} \qquad (2\text{-}7)$$

$$\text{Or } P_{ideal} = Pmeas + \frac{n^2 a}{V^2} \qquad (2\text{-}8)$$

The values of a and b in the van der Waals equation are constants, but are different depending on the gas. Table 2.1 below shows values of a and b for some gases.

Table 2.1: van der Waals constants for some gases

Gas	**a (L^2-atm/mol^2)**	**b (L/mol)**
He	0.03412	0.02370
Ne	0.2107	0.01709
H_2	0.2444	0.02661
Ar	1.345	0.03219
CH_4	2.253	0.04278
CO_2	3.592	0.04267
NH_3	4.170	0.03707

2.5.1 Derivation of the van der Waals equation

From the ideal gas law (equation 2-1), $PV = nRT$, van der Waals assumed that particles feel a net force between the particle and the container holding it. The density number of the particles, which is assumed to be uniform, is thus directly proportional to the net force.

$$C = \frac{N_A}{Vm} \tag{2-81}$$

where

N_A =number of particles,

Vm = volume excluded by a particle.

This net force is thus reduced by a factor which is assumed to be proportional to the square of the density number, and the pressure is thus reduced by P=a′C^2 .

Substituting C from equation (2-81) into P= a′C^2, we get

$$P = a'(Na/Vm)^2 \tag{2-82}$$

and substituting a = N_A^2a′ into equation (2-82), we obtain

$$P = \frac{a}{{V_m}^2} \tag{2-83}$$

The pressure is thus reduced by equation (2-83) in equation (2-84), shown below

$$P = \frac{RT}{Vm-b} - \frac{a}{Vm^2} \tag{2-84}$$

Rearranging equation (2.84) above and collecting similar terms, we get

$$(P + a/Vm^2)(Vm - b) = RT \tag{2-85}$$

Introducing n = number of moles into equation (2.85) and using the relationship $V = nv_m$, the van der Waals equation is derived as

$$\left(P + {an^2}/{v^2}\right)(V - nb) = nRT \tag{2-86}$$

2.5.2 Reduced Form

The van der Waals equation can be also written as

$$\left(P_R + \frac{3}{v_R^{\,2}}\right)\left(v_R - \frac{1}{3}\right) = \frac{8}{3}T_R \tag{2-9}$$

This form of the van der Waals equation can be used for all gases and liquids regardless of the values of the constants a and b depending on the gas involved. In equation (2-9),

$$P_R = \frac{P}{Pc} \text{ where } Pc = \frac{a'}{27b'^2} \tag{2-10}$$

$$v_R = \frac{v}{v_c} \text{ where } v_c = 3b' \tag{2-11}$$

$$T_R = \frac{T}{Tc} \text{ where } kTc = \frac{8a'}{27b'} \tag{2-12}$$

Pc, Vc, and Tc characterize the inflection point of the PV diagram. That is,

$$\left(\frac{\partial P}{\partial V}\right)_c = 0 \tag{2-13}$$

$$\left(\frac{\partial^2 P}{\partial V^2}\right)_c = 0 \qquad (2\text{-}14)$$

The equations (2-13) and (2-14), when solved for the van der Waals equation, yield the values of Pc, Vc, and Tc, and when they are substituted into the van der Waals equation, equation (2-9) is obtained.

This equation is explained using the "Theory of Corresponding States", which states that all gases and liquids, at related reduced temperature and reduced pressure, have the same compressibility factor and move away from behaving as an ideal gas to the same extent. When this happens, it can be said that the observed fluids have similar corresponding states regardless of the pressure, temperature, and volume of the individual fluids.

2.6 Further Explanation of Isothermal Plots.

An isotherm is a line that is drawn on a plot or graph and is used to link different points of constant temperature together.

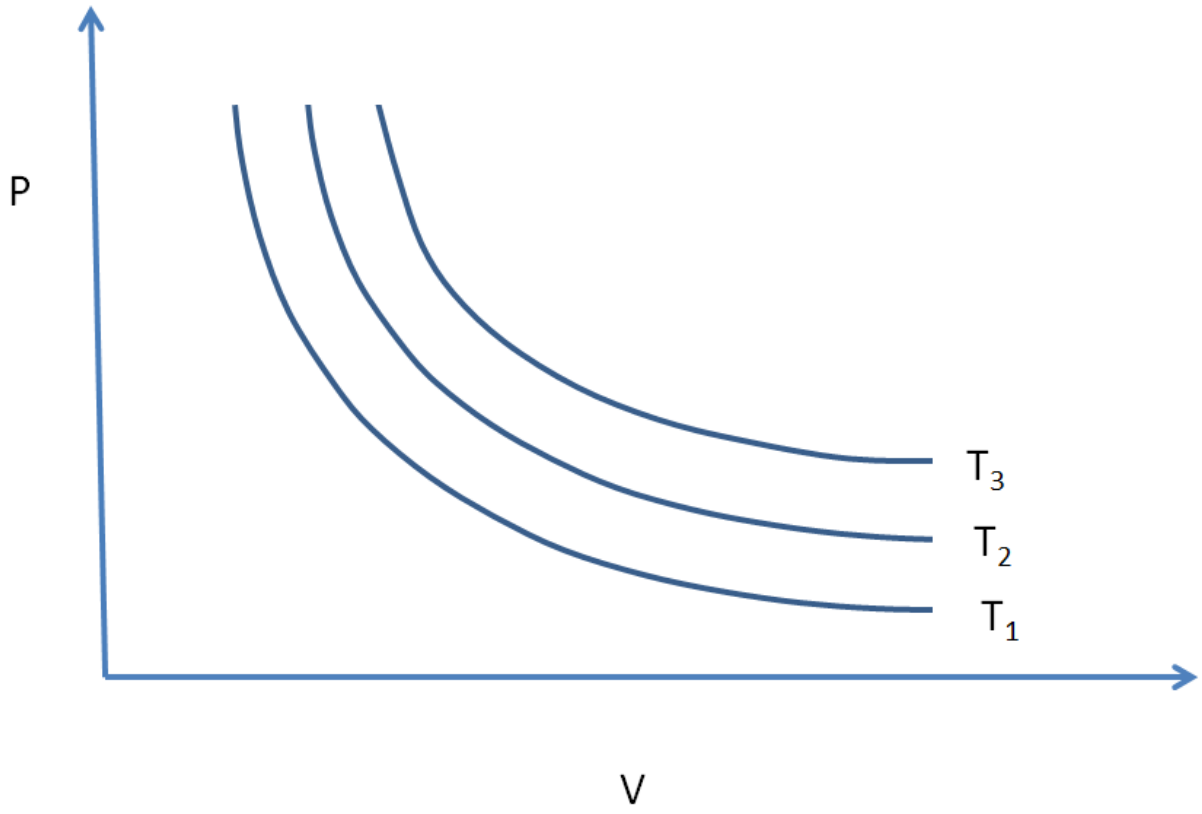

Figure 2.3: Isothermal plot for an ideal gas

Figure 2.3 above shows the isothermal plot for an ideal gas at constant PV; as the volume decreases, pressure increases, and as the pressure decreases, volume increases.

However, for a real gas, with the van der Waals equation of state the isothermal plot is different. To be able to plot the isothermal graph, a cubic equation of the van der Waals equation is used by considering equation (2-2):

$$\left(P + \frac{a}{v_2}\right)(v - b) = RT$$

Multiplying equation (2-2) by V^2 and rearranging, we get

$$PV^3 - (Pb + RT)V^2 + av - ab = 0 \qquad (2\text{-}15)$$

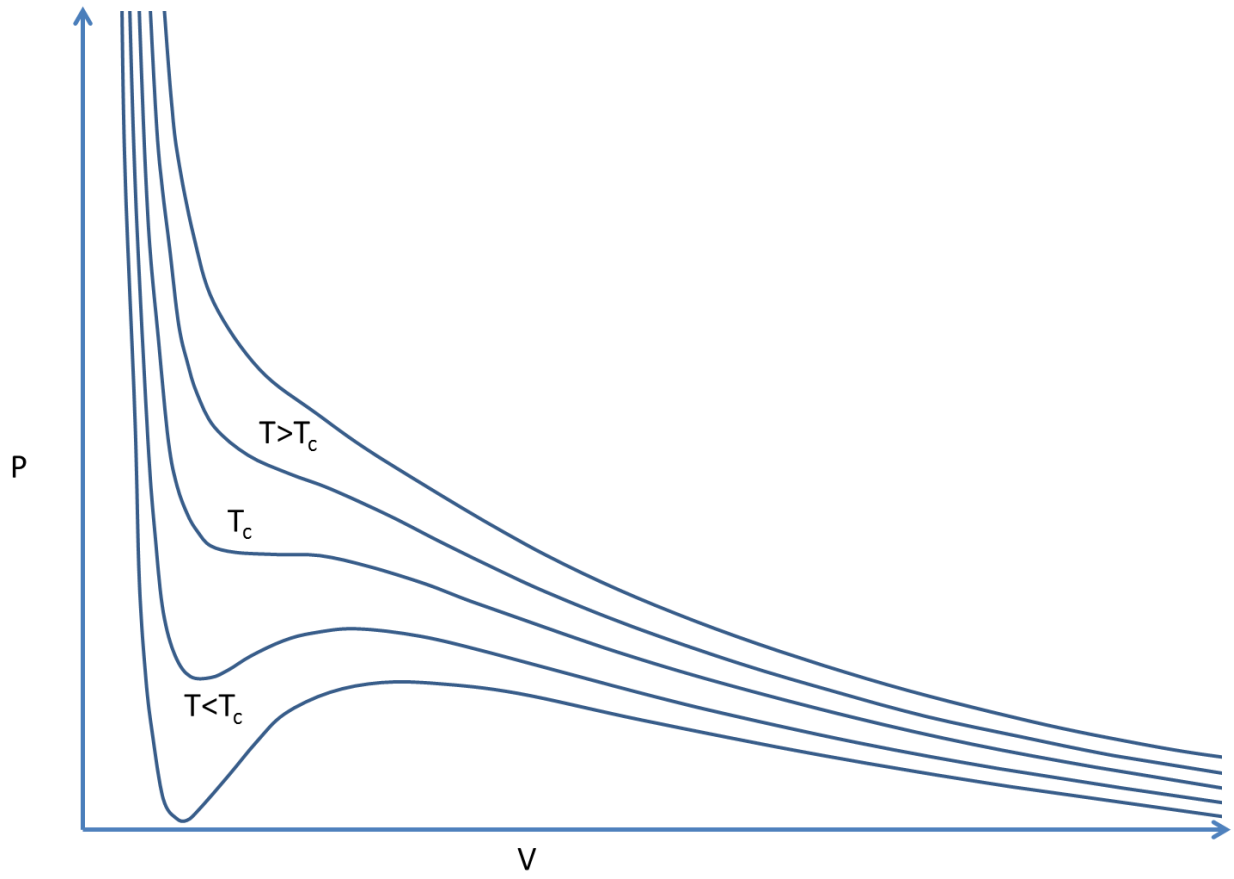

Figure 2.4: Isotherms for real gases.

Figure 2.4 above shows the isothermal plot for real gases at constant temperature and varying pressure and volume. From this figure it can be seen that at higher temperatures, the gas exhibits ideal gas behaviour and the isotherm is similar to that of an ideal gas. However, as temperature begins to decrease, there is a deviation from ideal gas to real gas and under these conditions, phase transitions occur. The two isotherms below Tc are considered unstable, and this is because at these stages, when volume decreases, the pressure does not increase.

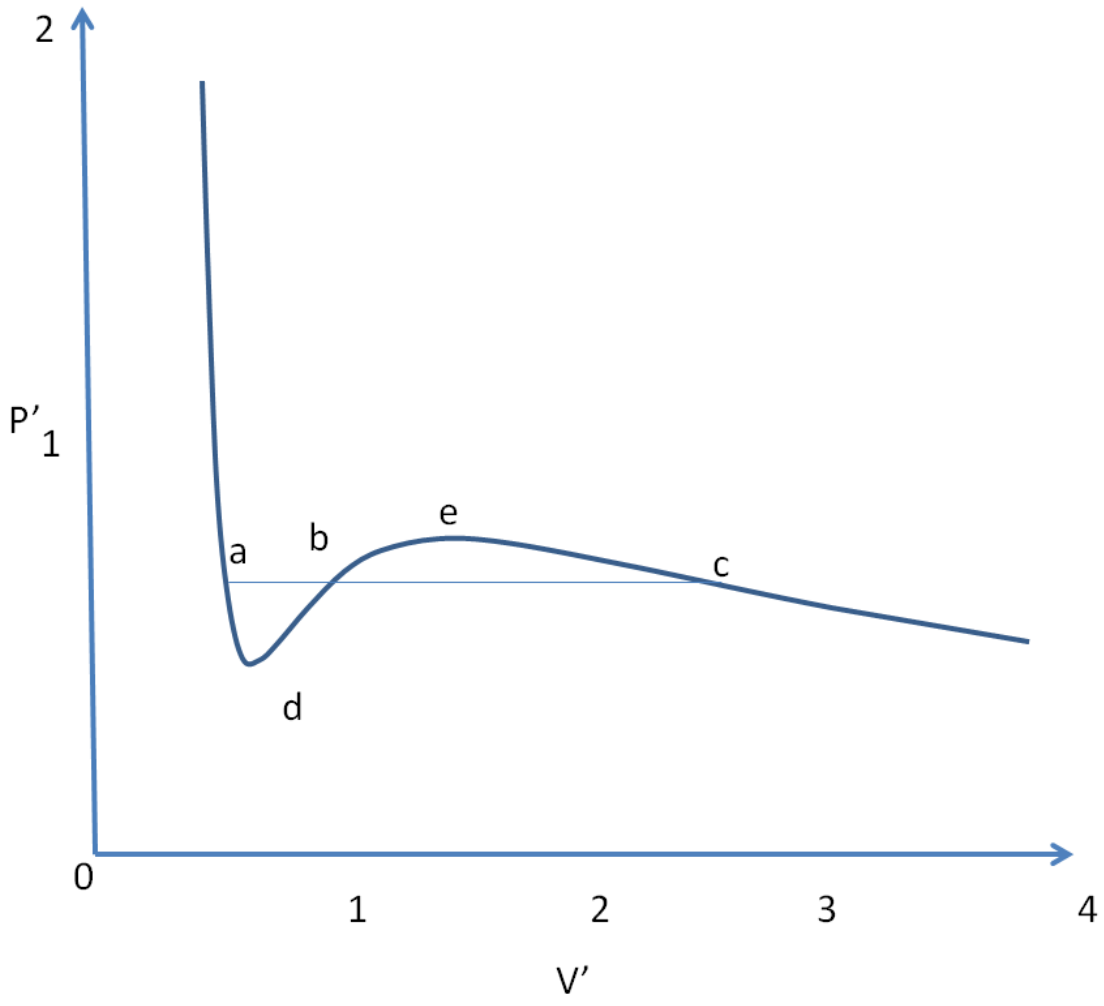

Figure 2.5 : a van der Waal isotherm

Figure 2.5 above takes a closer look at an isotherm below Tc. This helps in understanding what happens at this stage. At point (c), phase transition (gas condensation) is seen. At the area beyond point (c), pressure neither increases nor decreases as volume is decreased. Finally, as can be observed from Figure 5, equilibrium of the gas and liquid occurs between points (b) and (c). Point (d) is at the minimum while (e) is at the maximum. At point (a), the fluid is completely a liquid.

In the next chapter, we will review the fluid flow equations and will use the van der Waals equation presented here as the equation of state.

Chapter 3: Fluid flow equations

In this chapter, we present the equations that specify the fluid flow, and will simplify them for one-dimensional liquid vapour fluids.

3.1. The Euler equations

The Euler equations are the continuity and momentum equations for inviscid flows. They are simplified versions of the Navier -Stokes equations in the absence of viscosity terms. In conservation form, they may be written as

$$\frac{\partial \mathbf{m}}{\partial t} + \frac{\partial \mathbf{f}_x}{\partial x} + \frac{\partial \mathbf{f}_y}{\partial y} + \frac{\partial \mathbf{f}_z}{\partial z} = 0, \tag{3-1}$$

where,

$$\mathbf{m} = \begin{pmatrix} \rho \\ \rho u \\ \rho v \\ \rho w \\ E \end{pmatrix}; \tag{3-2}$$

$$\mathbf{f}_x = \begin{pmatrix} \rho u \\ p + \rho u^2 \\ \rho uv \\ \rho uw \\ u(E+p) \end{pmatrix}; \qquad \mathbf{f}_y = \begin{pmatrix} \rho v \\ \rho uv \\ p + \rho v^2 \\ \rho vw \\ v(E+p) \end{pmatrix}; \qquad \mathbf{f}_z = \begin{pmatrix} \rho w \\ \rho uw \\ \rho vw \\ p + \rho w^2 \\ w(E+p) \end{pmatrix}. \tag{3-3}$$

In the above equations, $\mathbf{m}$ is the vector of variables, $\mathbf{f}_x$, $\mathbf{f}_y$, and $\mathbf{f}_z$ are respectively flux vectors in x, y, and z directions, ρ is the density, u, v, and w are respectively velocity components in the x, y, and z directions, p is the pressure, and E is the energy.

The conservation form makes it clear that all components of the $\mathbf{m}$ vector are globally conserved. That is, the volume integrals of these quantities are constant in the domain if the effects of boundaries are cancelled; e.g., with periodic boundary conditions.

The equations may be also re-written in non-conservative form, as

$$\frac{\partial \mathbf{m}}{\partial t} + \mathbf{A}_x \frac{\partial \mathbf{m}}{\partial x} + \mathbf{A}_y \frac{\partial \mathbf{m}}{\partial y} + \mathbf{A}_z \frac{\partial \mathbf{m}}{\partial z} = 0. \tag{3-4}$$

where

$$\mathbf{A}_x = \frac{\partial \mathbf{f}_x(\mathbf{m})}{\partial \mathbf{m}} \quad , \quad \mathbf{A}_y = \frac{\partial \mathbf{f}_y(\mathbf{m})}{\partial \mathbf{m}} \quad , \quad \mathbf{A}_z = \frac{\partial \mathbf{f}_z(\mathbf{m})}{\partial \mathbf{m}}. \tag{3-5}$$

In this study, we focus on the one-dimensional case in which the continuity and x-momentum equations are simplified as

$$\begin{aligned} &\rho_t + (\rho u)_x = 0 \\ &u_t + u u_x + \frac{1}{\rho} p_x = 0 \end{aligned} \tag{3-6}$$

which can be re-written as

$$\rho_t + u\rho_x + \rho u_x = 0$$
$$u_t + uu_x + \frac{1}{\rho} p_x = 0 \tag{3-7}$$

Ignoring the nonlinear advection terms in the characteristic coordinates, and defining the specific volume as

$$\tau = \frac{1}{\rho}, \tag{3-8}$$

the equations are further simplified to

$$\tau_t - u_x = 0$$
$$u_t + p(\tau)_x = 0 \tag{3-9}$$

In van der Waals fluids, the governing conservation laws may be modified as:

$$\partial_t \tau - \partial_x u = 0,$$
$$\partial_t u + \partial_x p(\tau) = \grave{o}\partial_{xx} u - \alpha \grave{o}^2 \partial_{xxx} \tau, \tag{3-10}$$

where τ is the specific volume of the fluid, u is the velocity of the fluid, $\grave{o}$ and α are respectively the viscosity and dispersion (capillarity) coefficients, and p is the pressure. Note that the equations of motion have been linearized, since the system is assumed to be near critical.

3.2 Classification of the equations

Here we consider second-order linear PDEs, which have widespread applications. Their general form is given by

$$A\frac{\partial^2 u}{\partial x^2}+B\frac{\partial^2 u}{\partial x\partial y}+C\frac{\partial^2 u}{\partial y^2}+D=0 \tag{3-11}$$

These equations are divided into three categories, depending on the value of (B^2 - 4AC), as mentioned in Table 3.1.

Table 3.1: Classification of the second order linear PDEs

Condition	Equation type	Example
$B^2 - 4AC < 0$	**Elliptic PDE**	Laplace equation $\frac{\partial^2 T}{\partial x^2}+\frac{\partial^2 T}{\partial y^2}=0$
$B^2 - 4AC = 0$	**Parabolic PDE**	Contaminant transp. $\frac{\partial C}{\partial t}=K\frac{\partial^2 C}{\partial x^2}$
$B^2 - 4AC > 0$	**Hyperbolic PDE**	Wave equations $\frac{\partial^2 y}{\partial x^2}=\frac{1}{c^2}\frac{\partial^2 y}{\partial t^2}$

The Euler equations belong to the general family of signal-propagation equations, which are generally called hyperbolic equations. The solutions of hyperbolic equations are generally in the form of waves. That is, if any disturbance is added to the initial data of hyperbolic differential equations, then only a part of the time-space domain feels the disturbance. In other words, disturbances have a finite propagation speed relative to a fixed time coordinate. The information (disturbances) travels along special paths called characteristics of the equation. Due to this

feature, hyperbolic equations have a different behaviour than elliptic partial differential equations.

Elliptic operators are, on the other hand, a generalization of the Laplace operator. The coefficients of the highest-order derivatives are positive in these equations. This leads to an important property, which is that there are no real characteristic directions.

A popular method to solve elliptic equations is to add temporal variation terms to them and make them hyperbolic or parabolic. Then, the resulting equation is integrated in time until a steady state solution is obtained. A steady state implies that the temporal variation term is zero. Therefore, the obtained steady state solution is indeed a solution of the initial elliptic equation. Note that this also implies that in order to solve elliptic equations, only boundary conditions are required, as opposed to hyperbolic and parabolic equations which require initial conditions as well.

Although the above-mentioned definition of hyperbolic equations was given for second-order equations, it could be shown that a first-order equation or a system of first-order equations could be also hyperbolic.

The simplest form of hyperbolic equations is the advection equation (with real advection velocity), which implies that the initial disturbances are propagated in the flow direction (with the flow). The characteristic direction for this equation is basically the flow direction (Figure 3.1).

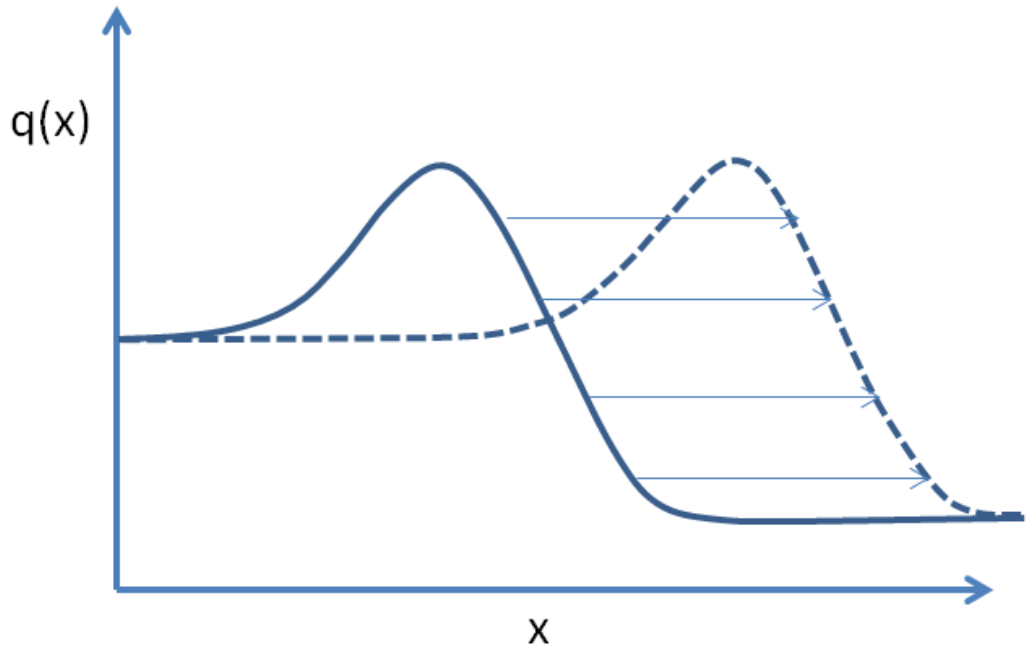

Figure 3.1: Advection of an initial disturbance with the flow

Similarly, a coupled system of first-order equations could be also hyperbolic if it could be reformulated as a set of decoupled advection equations. From a mathematical viewpoint, this means that the Jacobian matrix of the system should be diagonalisable, which in turn requires that the eigenvalues of the Jacobian matrix be real. If so, then these real eigenvalues play the role of advection velocity of the decoupled system. Note that in this case the parameters that are advected in the decoupled equations are not necessarily the same as those of the coupled system. In order to clarify this issue, we consider a set of linear equations written in the general form

$$\partial_t Q + A\partial_x Q = 0 \qquad (3\text{-}12)$$

where A is an $m \times m$ matrix and $Q = (q1..., qm)$ is a vector of m components. If A is already diagonal, the above system simply includes m decoupled advection equations which are each hyperbolic, and therefore the whole system is hyperbolic. If A is not diagonal, then the

equations are coupled. However, if A is diagonalisable, then this system of coupled equations could be decoupled, as explained below, and therefore the system is hyperbolic. In order for the matrix A to be diagonalisable, it must have m real eigenvalues. In that case, there exists a complete set of eigenvectors e_j, and then the vector Q can be decomposed on the basis of eigenvectors, as

$$Q = \sum_{i=1}^{m} \bar{q}_1 e_1 \tag{3-13}$$

and by definition of eigenvectors,

$$AQ = \sum_{i=1}^{m} \lambda_i \bar{q}_1 e_i \tag{3-14}$$

Let R be a matrix in which each column is one of the eigenvectors:

$$R = (e_1, ...e_m) \tag{3-15}$$

Then the system (3-12) can be written as

$$R^{-1}\partial_t Q + R^{-1} A R R^{-1} \partial_x Q = 0 \tag{3-16}$$

Defining

$$\bar{Q} = R^{-1} Q \tag{3-17}$$

and

$$\bar{A} = diag(\lambda_1, ..., \lambda_m) \tag{3-18}$$

the system (3-16) becomes

$$\partial_t \bar{Q} + \bar{A} \partial_x \bar{Q} = 0 \tag{3-19}$$

which represents m decoupled advection equations and is therefore hyperbolic.

Note that if the eigenvalues are not real, one cannot obtain the uncoupled set of equations, and the system will not be hyperbolic. The eigenvalues need not be necessarily different, and can be equal. In principle, the above system of equations has m sets of characteristics. However, typically, the number of characteristics is considered to be equal to the number of distinct characteristics.

Now let us consider a nonlinear system:

$$\partial_t Q + \partial_x F = 0 \tag{3-20}$$

where $F = (f_1, ..., f_m)$ can be a vector of nonlinear or linear functions, and therefore cannot be written as $F = AQ$. However, if F only depends on Q, then the system (3-20) can be written as

$$\partial_t Q + \frac{\partial F}{\partial Q} \partial_x Q = 0 \tag{3-21}$$

where $\frac{\partial F}{\partial Q}$ is called the Jacobian matrix.

If the Jacobian matrix has m real eigenvalues, then the system is again diagonalisable, and one obtains

$$\partial_t Q + \begin{bmatrix} \lambda_1 & & \\ & \ddots & \\ & & \lambda_m \end{bmatrix} {}_x Q = 0 \tag{3-22}$$

Again, one obtains n advection equations. However, this time the eigenvalues depend on Q, and therefore the equations are nonlinear. In general, the characteristics are not constant in time, and their value may change. Therefore, the shape of initial disturbances may change and

characteristics may converge and develop a shock wave, or may diverge and develop a rarefaction wave, as shown in Figure 3.2.

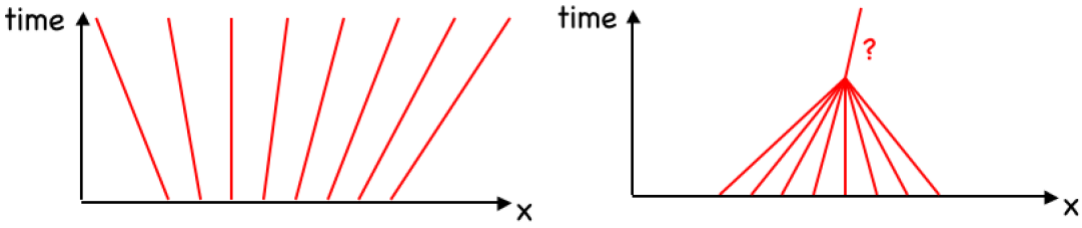

Figure 3.2: Diverging characteristics lead to rarefaction (left), and converging characteristics may lead to shock waves (right)

A familiar example of nonlinear hyperbolic equations is the system of shallow water equations, and a well-known problem is the dam-break case, or the general Riemann problem, which develops both shock waves and rarefactions, as shown in Figures 3.3 and 3.4.

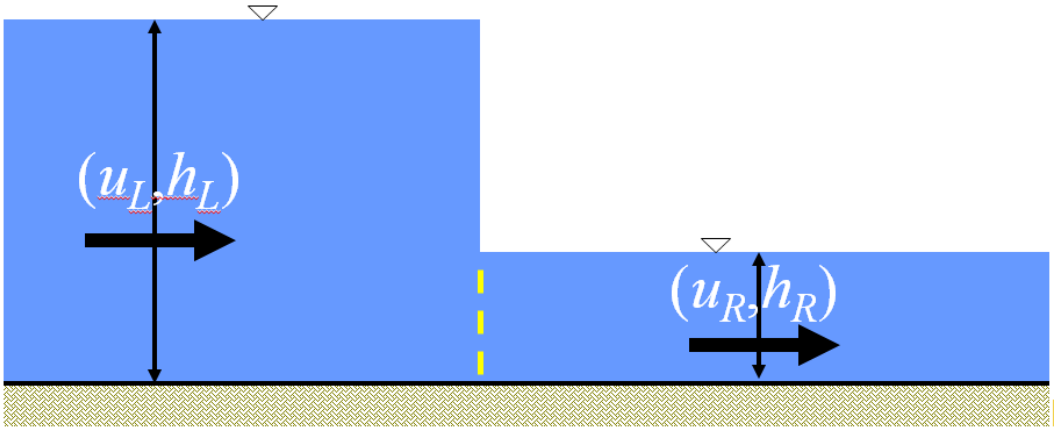

Figure 3.3: Initial conditions of the Riemann Problem

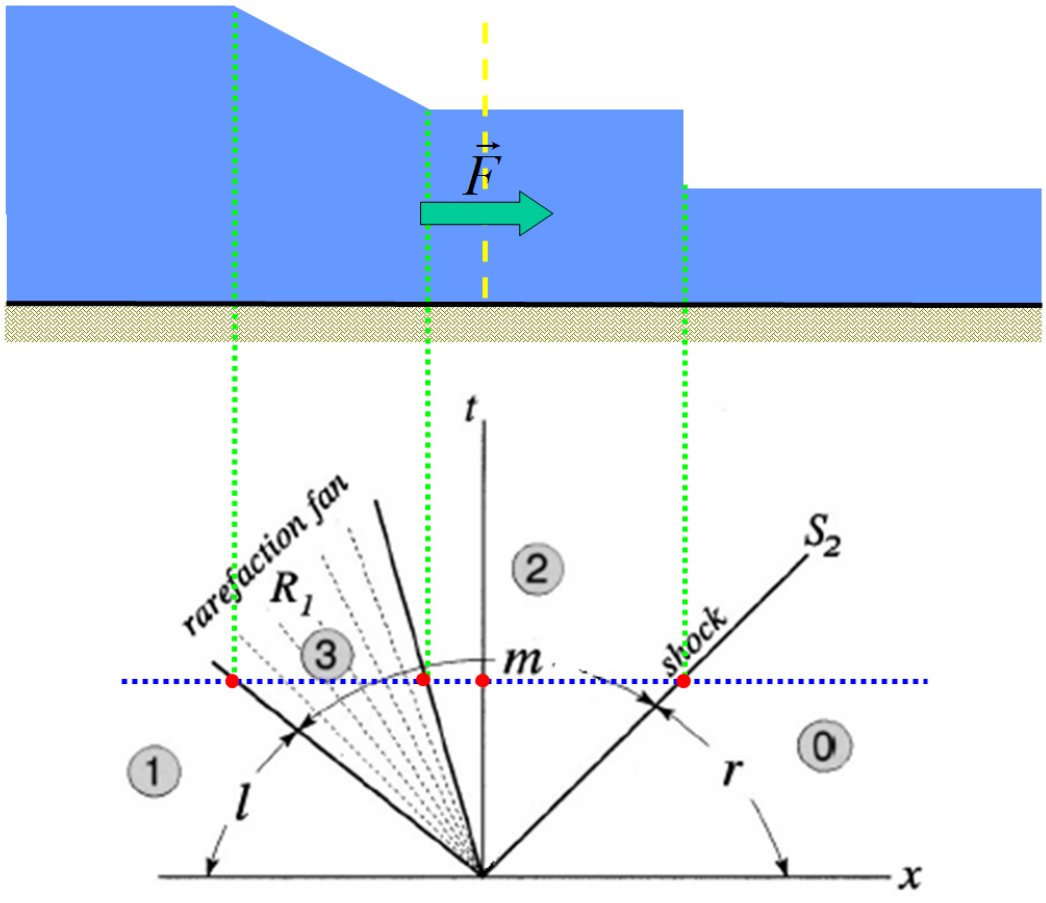

Figure 3.4: Typical Solution of the Riemann problem

Finally, let us here explain why a system with imaginary eigenvalues is not hyperbolic, via a simple example. Consider the system

$$\begin{aligned} &\partial_t q_1 + \partial_x q_2 = 0, \\ &\partial_t q_2 - \partial_x q_1 = 0 \end{aligned} \tag{3-23}$$

or

$$\partial_t \begin{pmatrix} q_1 \\ q_2 \end{pmatrix} + \begin{pmatrix} 0 & 1 \\ -1 & 0 \end{pmatrix} \partial_x \begin{pmatrix} q_1 \\ q_2 \end{pmatrix} = 0, \tag{3-24}$$

The eigenvalues of the Jacobian matrix are $\pm i$ and therefore the system is not hyperbolic. This can be confirmed by combining the two equations, which leads to

$$\partial^2_t q_1 + \partial^2_x q_1 = 0 \tag{3-25}$$

This is clearly a Laplace equation, which is a well-known example of elliptic equations. Therefore, in summary, if the eigenvalues of the Jacobian matrix are not all real, the system will be elliptic. This is the case for the liquid-vapor flows in near critical temperatures for certain cases, as explained in the following section.

3.3. The pressure function

As mentioned previously, pressure can be expressed as a function of the specific volume of the fluid $p = p(\tau)$ defined for $\tau > 0$:

$$\begin{aligned} &\lim_{\tau \to 0} p(\tau) = +\infty, \\ &\lim_{\tau \to +\infty} p(\tau) = 0, \end{aligned} \tag{3-26}$$

and there exist two positive numbers, a and c, such that $0 < a < c$, and

$$\begin{aligned} &p''(\tau) > 0, \quad \tau \in (0, a) \cup (c, +\infty), \\ &p''(\tau) < 0, \quad \tau \in (a, c), \\ &p'(a) > 0. \end{aligned} \tag{3-27}$$

As mentioned above, in the absence of diffusion and dispersion terms the system (3-10) has a mixed elliptic-hyperbolic behaviour. Assuming that there exist two positive numbers d and e such that

$$p'(d) = p'(e) = 0 \tag{3-28}$$

and $0 < d < a < e < c$, then this system is elliptic for $d < \tau < e$, where $p'(\tau)$ is positive, and otherwise it is hyperbolic. Note that $p'(\tau)$ is negative in the hyperbolic regime, and the system in that case has two left- and right-wave speeds, given by $\sqrt{-p'(\tau)}$ and $-\sqrt{-p'(\tau)}$

As mentioned previously, from a mathematical viewpoint the van der Waals system is a very special one because the pressure function has two inflection points.

In a series of numerical experiments, LeFloch and Mohammadian (2008) showed that the solutions of the van der Waals system are not unique, and that the system may have several solutions. Indeed, the kinetic function for this system may be non-monotonic and non-single-valued (LeFloch and Mohammadian, 2008). That is, multiple intermediate states can exist for a given right-side state of the Riemann problem.

In this project, as in LeFloch and Mohammadian (2008), a pressure equation is used which has the same form as

$$p(\tau) := \frac{RT}{(\tau - \frac{1}{3})} - \frac{3}{\tau^2} \qquad (3\text{-}29)$$

with $R = \frac{8}{3}$ and $T = 1.005$.

As shown in Figure 3.4, this flux function has two inflection points, at $\tau = 1.00996$ and 1.8515.

Note that in the above equation, the variables (i.e., specific volume, temperature, and pressure) denote their reduced value; i.e., their ratio with their critical value.

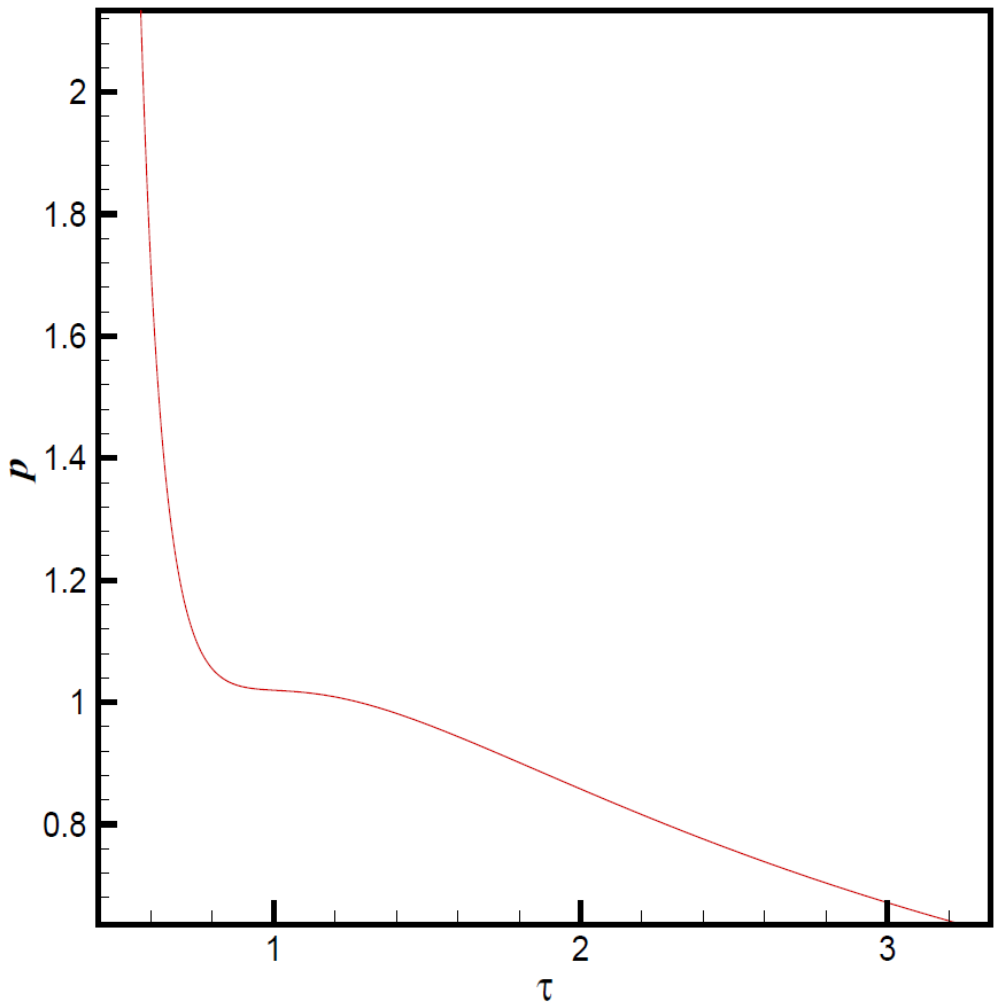

Figure 3.4: van der Waals flux function

The solutions of the Riemann problem for the van der Waals system were numerically studied in LeFloch and Mohammadian (2008) with the above pressure function. They identified three different regimes. In the first regime (regime A), a stationary shock wave is produced at the center, where the initial discontinuity is located. In the second regime (regime B), a non-classical left-going non-stationary shock wave is generated. By increasing the velocity at the left-hand state of the Riemann problem, the shock wave speed decreases, and the kinetic function in this case is neither single-valued nor monotonic. In the third regime (regime C), a non-classical, non-

stationary, left-going shock wave is generated. The left and right states of this shock wave are constant and are equal to the limiting values of regime B.

3.4. The research methodology

The research methodology in this project is mainly experimental. We will consider several numerical schemes and will examine their performance in numerical simulation of shock waves in van der Waals fluids. Our criteria to compare various numerical methods will be the presence and level of numerical oscillations. We will consider the high order finite difference schemes studied in LeFloch and Mohammadian (2008) as reference solutions. In that study it was concluded that as the order of the accuracy of the finite difference methods increases, their results become more accurate and their kinetic function becomes closer to the analytical kinetic function. Therefore, we consider the limiting solution of high order finite difference schemes as the reference solution and will be looking for a numerical method that leads to a lower level of numerical oscillations and leads to a solution closer to the limiting solution obtained by high order finite difference methods. As we will numerically show, the Chebyshev pseudospectral method is the most accurate method among all schemes considered in this project.

Chapter 4: Numerical method

The system (3-10) will be considered in this chapter. This system includes temporal and spatial derivatives. In this chapter, we present the numerical method for spatial discretization and temporal integration.

Our general approach in solving the equation (3-10) will be a semi-discretization approach. That is, we will discretize the equations in space and will keep the temporal derivatives. For space discretization scheme, we begin with the Chebyshev pseudospectral method in this chapter and will later consider other schemes in Chapter 6. This approach will convert the partial differential equations to ordinary differential equations because only temporal derivatives will remain in the system. The resulting (semi-discrete) ordinary differential equations could be then solved using any temporal integration scheme for ordinary differential equations. For temporal integration, we will use the standard fourth order Runge-Kutta method. Again in Chapter 6, we will examine the impact of temporal differentiation scheme by using the eighth order Runge-Kutta method and the Crank-Nicolson schemes. As we will show later, the impact of temporal differentiation scheme is less significant than the spatial discretization method and the fourth order Runge-Kutta method is a suitable choice for temporal integration.

4.1 Space discretization scheme

In this project we use the Gauss-Chebyshev-Lobatto (GCL) points for the positioning of unevenly-spaced grid points for polynomial expansion:

$$x_j = cos(j\pi / N), \qquad j = 0,1,...,N \tag{4-1}$$

These points are the projections of equi-spaced points on the upper half of the unit circle onto $[-1,1]$ over $N+1$ grid points. Note that in usual Fourier methods an even number of grid points is used. However, with Chebyshev polynomials, N could be odd or even.

The numerical derivative of a grid function (here, the numerical flux) defined on the GCL points is calculated in two steps in the Chebyshev spectral method. In the first step, given the grid function on the Chebyshev points, the unique polynomial p of degree $\leq N$ is constructed such that

$$p(x_j) = \omega_j, \quad j = 0,\ldots,N \tag{4-2}$$

where

$$\omega_j = \omega(x_j) \tag{4-3}$$

The derivative of this polynomial $p'(x)$ is calculated on grid points in the second step. As an essential feature of the Chebyshev polynomial method, the two steps can be efficiently combined in a single matrix form in order to calculate the derivative at grid points

$$p'_N = D_N \omega, \tag{4-4}$$

where

$$p'_N = \left(p'(x_0), p'(x_0),\ldots, p'(x_N)\right) \tag{4-5}$$

$$\omega = \left(\omega(x_0), \omega(x_1),\ldots, \omega(x_N)\right) \tag{4-6}$$

and D_N is the *Chebyshev spectral differential matrix*; an $(N+1)\times(N+1)$ matrix given by

$$D_N = \begin{bmatrix} (D_N)_{00} & (D_N)_{01} & \cdots & \cdots & (D_N)_{0N} \\ (D_N)_{10} & (D_N)_{11} & \cdots & \cdots & (D_N)_{1N} \\ \vdots & \vdots & \ddots & \vdots & \\ (D_N)_{N0} & (D_N)_{N1} & \cdots & \cdots & (D_N)_{NN} \end{bmatrix} \tag{4-7}$$

where

$$(D_N)_{00} = \frac{2N^2+1}{6} \tag{4-8}$$

$$(D_N)_{NN} = -\frac{2N^2+1}{6} \tag{4-9}$$

$$(D_N)_{jj} = \frac{-x_j}{2(1-x_j^2)}$$

$$j = 1,...,N-1 \tag{4-10}$$

$$(D_N)_{ij} = \frac{c_i}{c_j}\frac{(-1)^{i+j}}{(x_i - x_j)},$$

$$i \neq j, \qquad i, j = 0,...,N \tag{4-11}$$

with

$$c_i = \begin{cases} 2, & i = 0 \quad or \quad N, \\ 1, & otherwise. \end{cases} \tag{4-12}$$

Note that the jth column of D_N corresponds to the derivative of polynomial interpolant $p_j(x)$ of degree N to the delta function supported at x_j, which is sampled at the GCL points x_j (Trefethen, 2000). For $N = 2$, the differentiation matrix becomes

$$D_2 = \begin{bmatrix} \frac{3}{2} & -2 & \frac{1}{2} \\ \frac{1}{2} & 0 & -\frac{1}{2} \\ -\frac{1}{2} & 2 & -\frac{3}{2} \end{bmatrix} \tag{4-13}$$

where its first, second, and third rows, respectively, represent standard second-order forward, centered, and backward finite difference schemes. The coefficients of higher-order Chebyshev spectral differentiation matrices also represent high-order finite difference methods on uneven grids. This is due to the fact that the Chebyshev method is a polynomial expansion over GCL points, and the polynomial expansions are unique.

The off-diagonal entries of D_N are calculated using (4-11). However, the diagonal components are calculated using an alternative formula:

$$(D_N)_{ii} = -\sum_{\substack{j=0 \\ j\neq i}}^{N} (D_N)_{ij} \tag{4-14}$$

This method reduces the instability of calculations due to rounding errors (Baltensperger & Berrut, 1999; Bayliss et al., 1994). A derivation of (4-11) can be found in Trefethen (2000).

Note that the position of the GCL points and the corresponding matrix D_N do not change with time, and therefore need to be calculated only once, at the beginning of calculations. Although the above formulas are given for the interval $[-1,1]$, by a simple change of variables they could be also used for an interval $[0,L]$. In this project, the above procedure is used for calculation of flux derivatives in the van der Waals system. However, the derivatives required to calculate the fluxes are obtained using the standard centered fourth-order finite difference scheme.

4.2 Time Marching Algorithm

In this project, a Runge-Kutta scheme is employed for time integration of the semi-discretized system. For a vector $U(t)$ defined by $U(t) = (u_i(t))_{i=\ldots,-1,0,1,\ldots}$, the semi-discretized scheme may be written as

$$\frac{dU}{dt} = R[U(t)] \tag{4-15}$$

where $R[U(t)]$ is the right-hand side of the van der Waals system discretized using either a finite difference or a Chebyshev pseudospectral method. The resulting system of ordinary differential equations may be numerically solved by an s -stage Runge-Kutta scheme, given by

$$\begin{aligned} g^k &= R\left(U^n + \Delta t \sum_{j=1}^{k-1} a_{k,j} g^j\right), \\ U^{n+1} &:= U^n + \Delta t \sum_{k=1}^{s} b_k g^k. \end{aligned} \tag{4-16}$$

In this study, a fourth-order Runge-Kutta scheme is used for temporal integration for which the non-zero coefficients are given by:

$$a_{2,1} = 1/2, a_{3,2} = 1/2, a_{4,3} = 1, b_1 = 1/6, b_2 = 1/3, b_3 = 1/3, b_4 = 1/6. \tag{4-17}$$

Here, we also use the finite difference method used by LeFloch and Mohammadian (2008) in order to evaluate the performance of the Chebyshev pseudospectral method. The corresponding discretized forms are briefly reviewed here.

We represent the grid points by x_i and the approximated solution at those grid points by u_i. Also, f_i corresponds to the value of the flux function at the grid points $f(u_i)$. The semi-discrete schemes for the grid functions $u_i = u_i(t)$ can be calculated with these notations by using standard finite difference methods or the pseudospectral scheme as given in the following. The 4th-order finite difference is written as

$$\begin{aligned}\frac{du_i}{dt} &= -\frac{1}{h}\left(\frac{1}{12}f_{i-2} - \frac{2}{3}f_{i-1} + \frac{2}{3}f_{i+1} - \frac{1}{12}f_{i+2}\right) \\ &+ \frac{\grave{o}}{h}\left(-\frac{1}{12}u_{i-2} + \frac{4}{3}u_{i-1} - \frac{5}{2}u_i + \frac{4}{3}u_{i+1} - \frac{1}{12}u_{i+2}\right) \\ &+ \frac{\alpha\grave{o}^2}{h}\left(-\frac{1}{2}u_{i-2} + u_{i-1} - u_{i+1} + \frac{1}{2}u_{i+2}\right),\end{aligned} \tag{4-18}$$

where h represents the grid size. It should be mentioned that the above system is fully conservative, e.g., with periodic boundary conditions. That is, $\sum_i u_i(t)$ does not change in the absence of boundary effects.

For completeness, the employed higher-order finite difference methods are also presented in the following.

The 4th-order discretization method is given by

$$f_x = \frac{1}{12}f_{i-2} - \frac{2}{3}f_{i-1} + \frac{2}{3}f_{i+1} - \frac{1}{12}f_{i+2} \tag{4-19}$$

the 6th-order discretization scheme leads to

$$f_x = -\frac{1}{60}f_{i-3} + \frac{3}{20}f_{i-2} - \frac{3}{4}f_{i-1} + \frac{3}{4}f_{i+1} - \frac{3}{20}f_{i+2} + \frac{1}{60}f_{i+3} \tag{4-20}$$

the 8th-order finite difference method has the following form

$$\begin{aligned}f_x &= \frac{1}{280}f_{i-4} - \frac{4}{105}f_{i-3} + \frac{1}{5}f_{i-2} - \frac{4}{5}f_{i-1} \\ &+ \frac{4}{5}f_{i+1} - \frac{1}{5}f_{i+2} + \frac{4}{105}f_{i+3} - \frac{1}{280}f_{i+4},\end{aligned} \tag{4-21}$$

and the 10th-order finite difference method leads to

$$\begin{aligned}f_x &= \frac{-1}{1260}f_{i-5} + \frac{5}{504}f_{i-4} - \frac{5}{84}f_{i-3} + \frac{5}{21}f_{i-2} - \frac{5}{6}f_{i-1} \\ &+ \frac{5}{6}f_{i+1} - \frac{5}{21}f_{i+2} + \frac{5}{84}f_{i+3} - \frac{5}{504}f_{i+4} + \frac{1}{1260}f_{i+5}.\end{aligned} \tag{4-22}$$

Chapter 5: Numerical Experiments

Here, two numerical experiments are performed to verify the performance of the pseudospectral method. In the first test, the left and right states correspond to the hyperbolic-elliptic regime, while the second test case deals with the performance of the scheme in the elliptic regime. In both test cases, boundaries are located far enough away that the waves do not reach them, and the influence of boundaries is thus avoided.

In the following test cases, the equation (3.10) will be solved which is repeated here

$$\begin{aligned} &\partial_t \tau - \partial_x u = 0, \\ &\partial_t u + \partial_x p(\tau) = \text{ò}\partial_{xx} u - \alpha \text{ò}^2 \partial_{xxx} \tau, \end{aligned} \tag{5.1}$$

The above system includes simplified continuity and momentum equations for van der Waals fluids.

5.1. Test 1

In the first test case we consider a Riemann problem with the following left- and right-hand states:

$$u_L = 1.05, \qquad \tau_L = 0.8 \tag{5-2}$$

$$u_R = 1, \qquad \tau_R = 2 \tag{5-3}$$

where subscripts R and L respectively represent right- and left-hand states. With the above values, the two inflection points of the pressure function are between the left- and right-hand states. The numerical modelling is conducted up to t=0.065 with a time-step of 0.000042 (non-

dimensional units) and 700 grid points. The viscosity and dispersion coefficients were fixed to $\grave{o} = 3 \times 10^{-5}$ and $\alpha = 10$ for all schemes. A sensitivity analysis regarding these parameters will be presented in the following.

The above initial values lead to a right-going classical shock wave and a left-going rarefaction followed by a left-going non-classical shock wave, which makes this test case a challenging one for numerical methods.

Figures 5.1 to 5.5 show the velocity and specific volume profiles calculated by the second-, fourth-, sixth-, eighth-, and tenth-order finite difference schemes respectively.

The second-order scheme, as observed in Figure 5.1, leads to a high level of numerical oscillations. Moreover, the distinct intermediate region is not well-represented in this scheme.

The numerical oscillations are reduced and become smaller as the order of accuracy increases, as was also reported in LeFloch and Mohammadian (2008).

All schemes lead to two fast noise structures going towards the left- and right-hand boundaries ahead of the rarefaction and shock waves. The results of the Chebyshev pseudospectral method are shown in Figure 5.6. The pseudospectral method performs better than all other employed finite difference schemes and does not lead to fast short-wave noise packages which move to the right- and left-hand sides. Such an improvement in the results can be justified by the fact that the order of accuracy of the pseudospectral method is much higher than that of all other employed finite difference schemes. These results confirm the conjecture proposed in LeFloch and Mohammadian (2008), which stated that the numerical solution converges with the analytical one by increasing the order of accuracy.

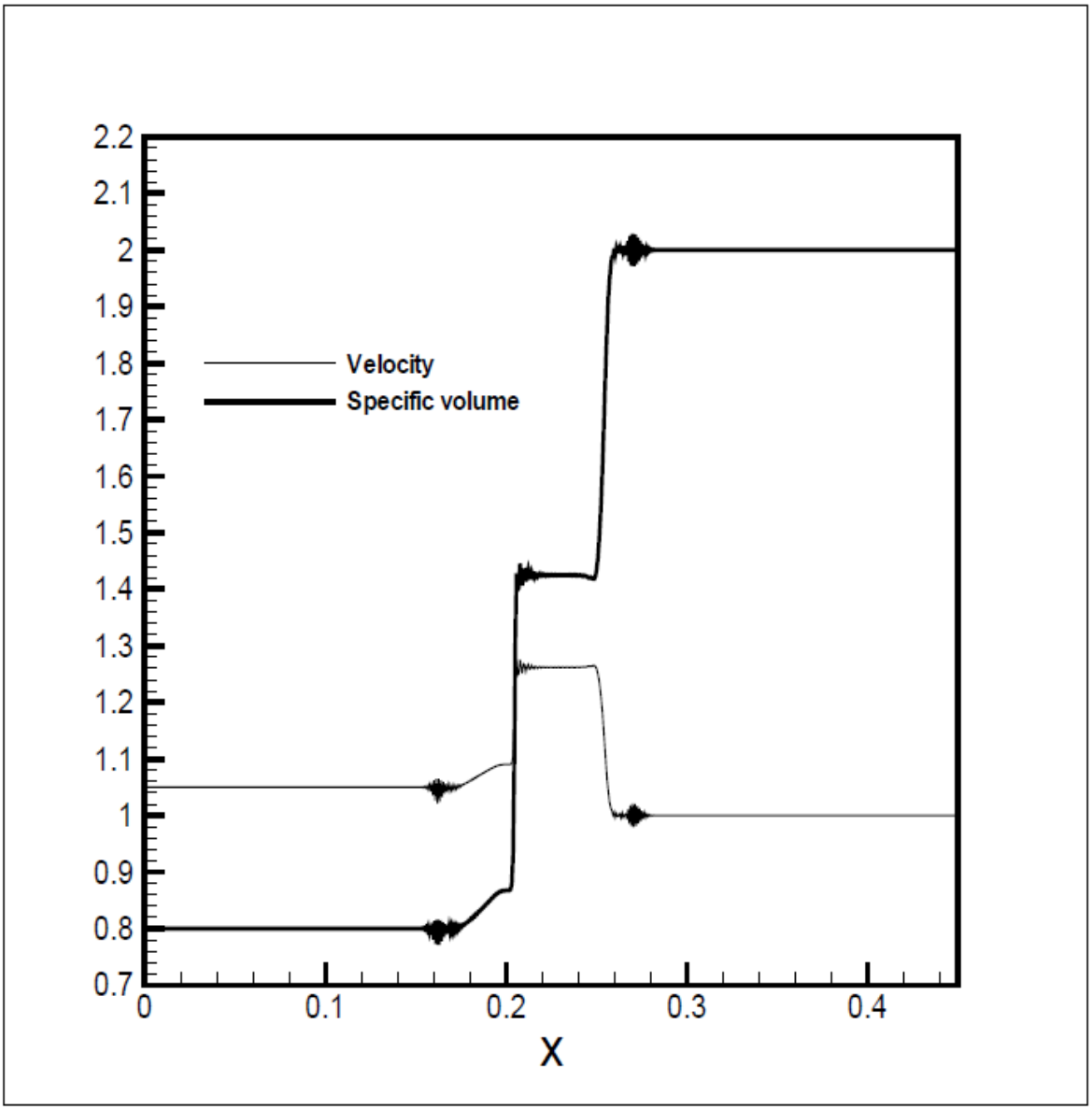

Figure 5.1: Velocity field and specific volume profile using the 2nd-order finite difference method

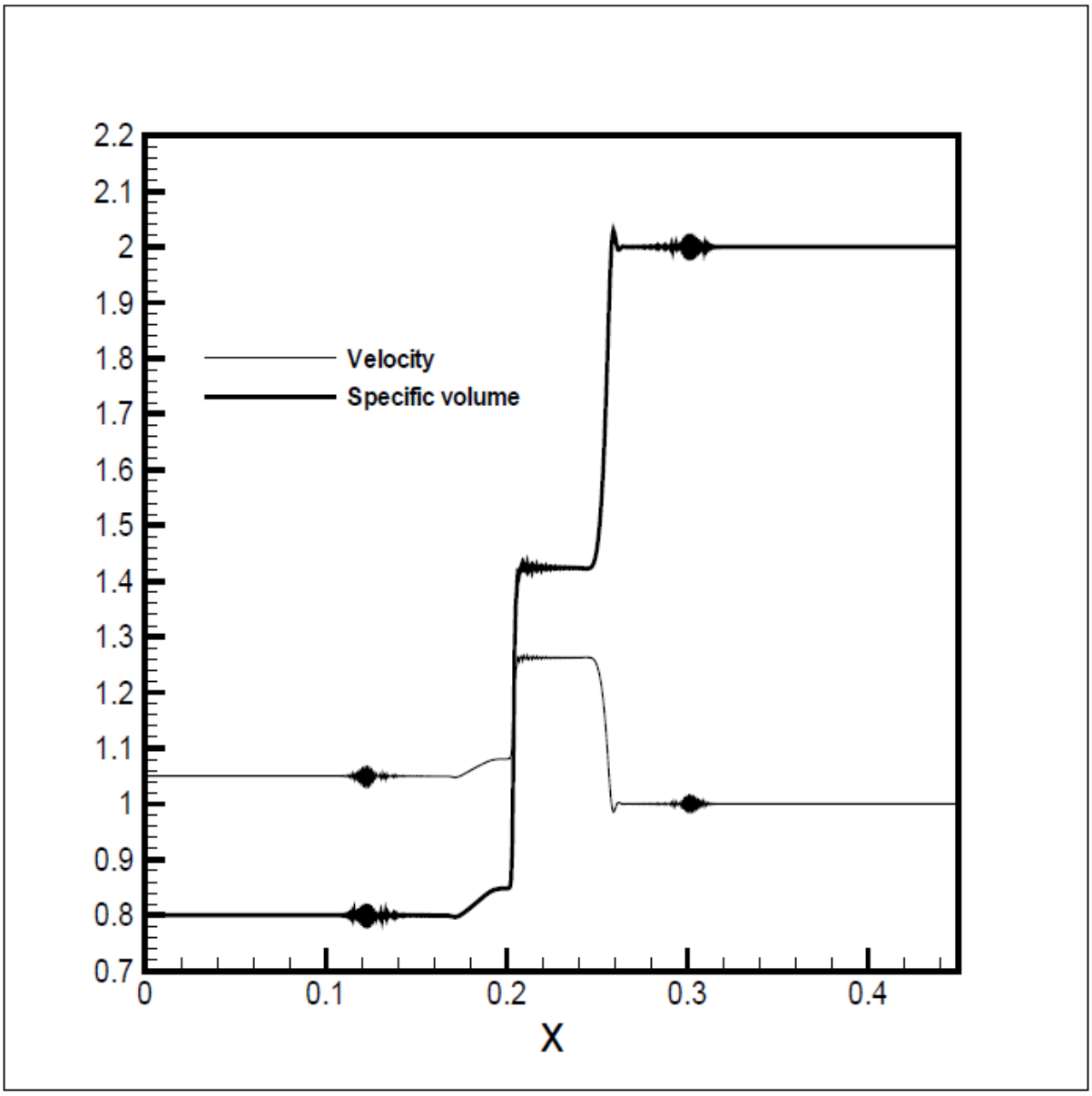

Figure 5.2: Velocity field and specific volume profile using the 4th-order finite difference method

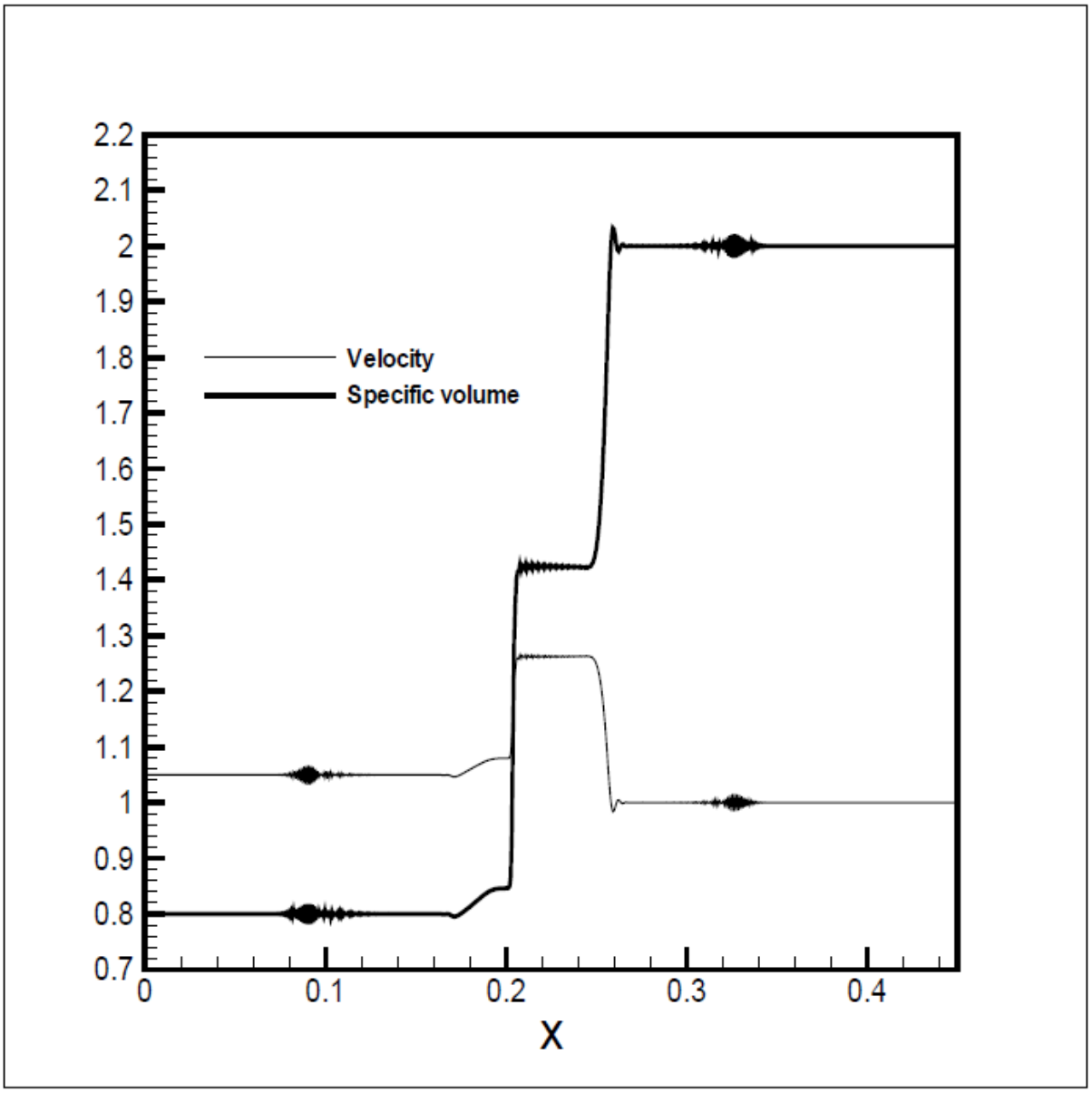

Figure 5.3: Velocity field and specific volume profile using the 6th-order finite difference method

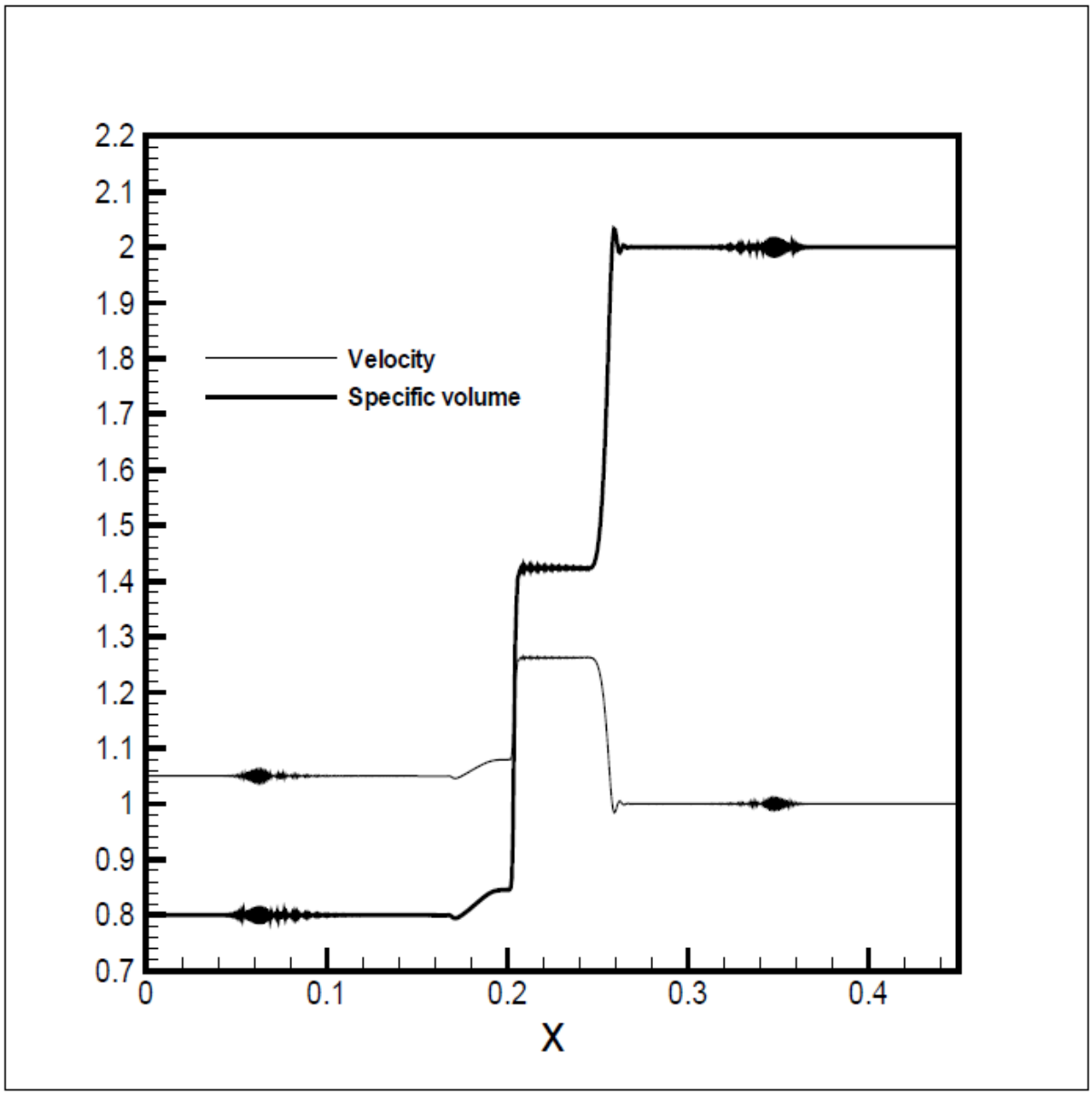

Figure 5.4: Velocity field and specific volume profile using the 8th-order finite difference method

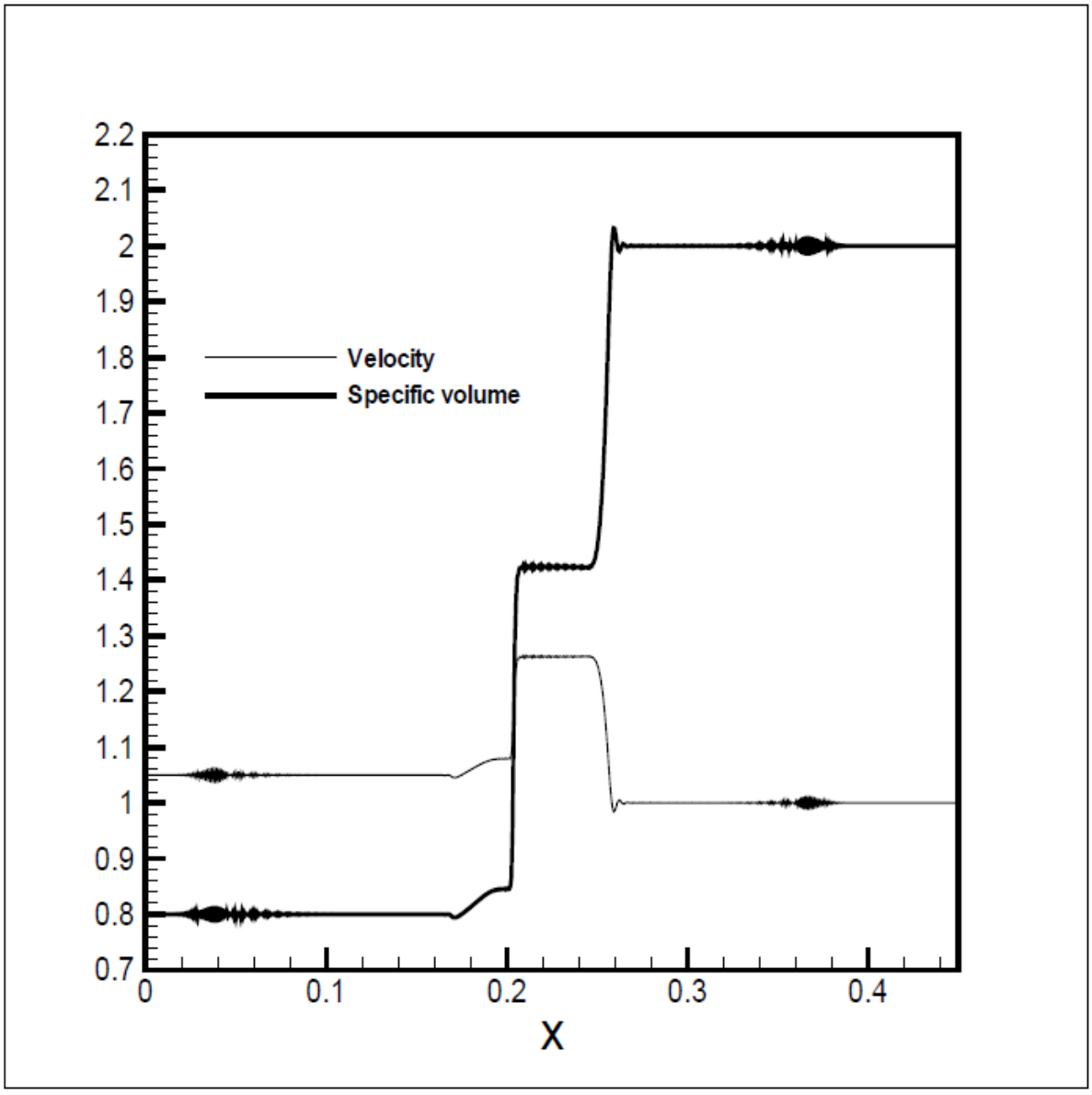

Figure 5.5: Velocity field and specific volume profile using the 10th-order finite difference method

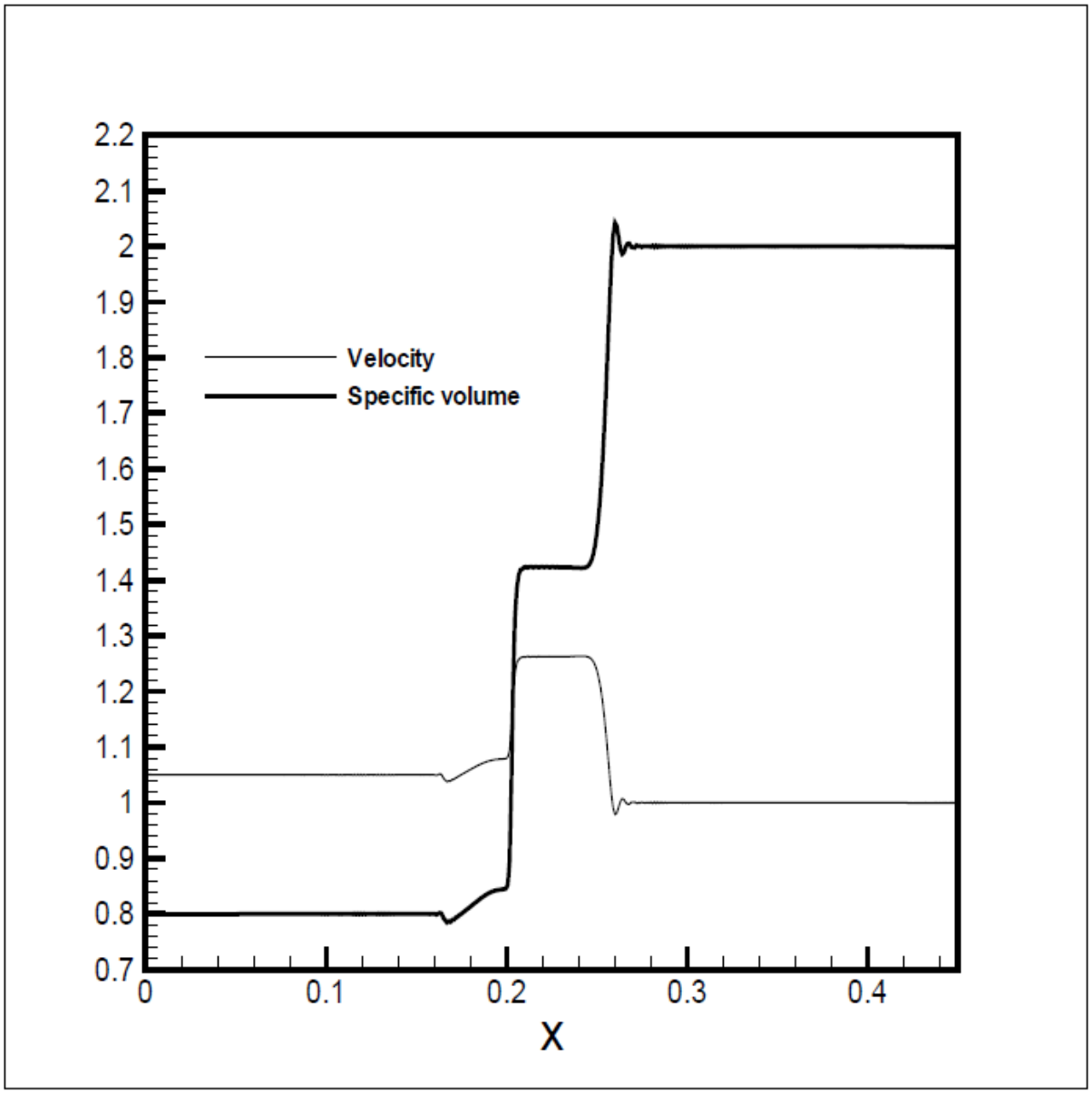

Figure 5.6: Velocity field and specific volume profile using the Chebyshev pseudospectral method

In order to observe the impact of the viscosity and dispersion coefficient, a sensitivity analysis was performed. The value of the velocity at the middle state is shown in Figure 5.7, where the dispersion coefficient is kept constant at $\alpha = 10$ and the viscosity coefficient is variable.

It is clear from this figure that the results of all schemes converge as the viscosity coefficient increases, and the value of $\grave{o} = 5 \times 10^{-5}$ may be considered as the typical value at which the results of higher-order schemes become very close.

It is also observed that as the order of accuracy increases, the numerical methods converge, and the Chebyshev pseudospectral scheme is the closest one to the limiting value. The fast noise structures are always present in the results of finite difference schemes (not shown), which is not the case for the Chebyshev pseudospectral method.

Similar behaviour is observed for $\alpha = 5$ and $\alpha = 1$, although the value of the intermediate state depends on α. Therefore, it can be concluded that the Chebyshev pseudospectral method performs better than the other schemes over a large range of diffusion and dispersion coefficients.

Finally, it should be mentioned that in order to reduce dispersive oscillations within a finite-difference approach, a change of variables was proposed in Cockburn and Gau (1996), and more recently in Pecenko et al. (2010). This approach may be also possible with the Chebyshev pseudospectral method and is the subject of a future study.

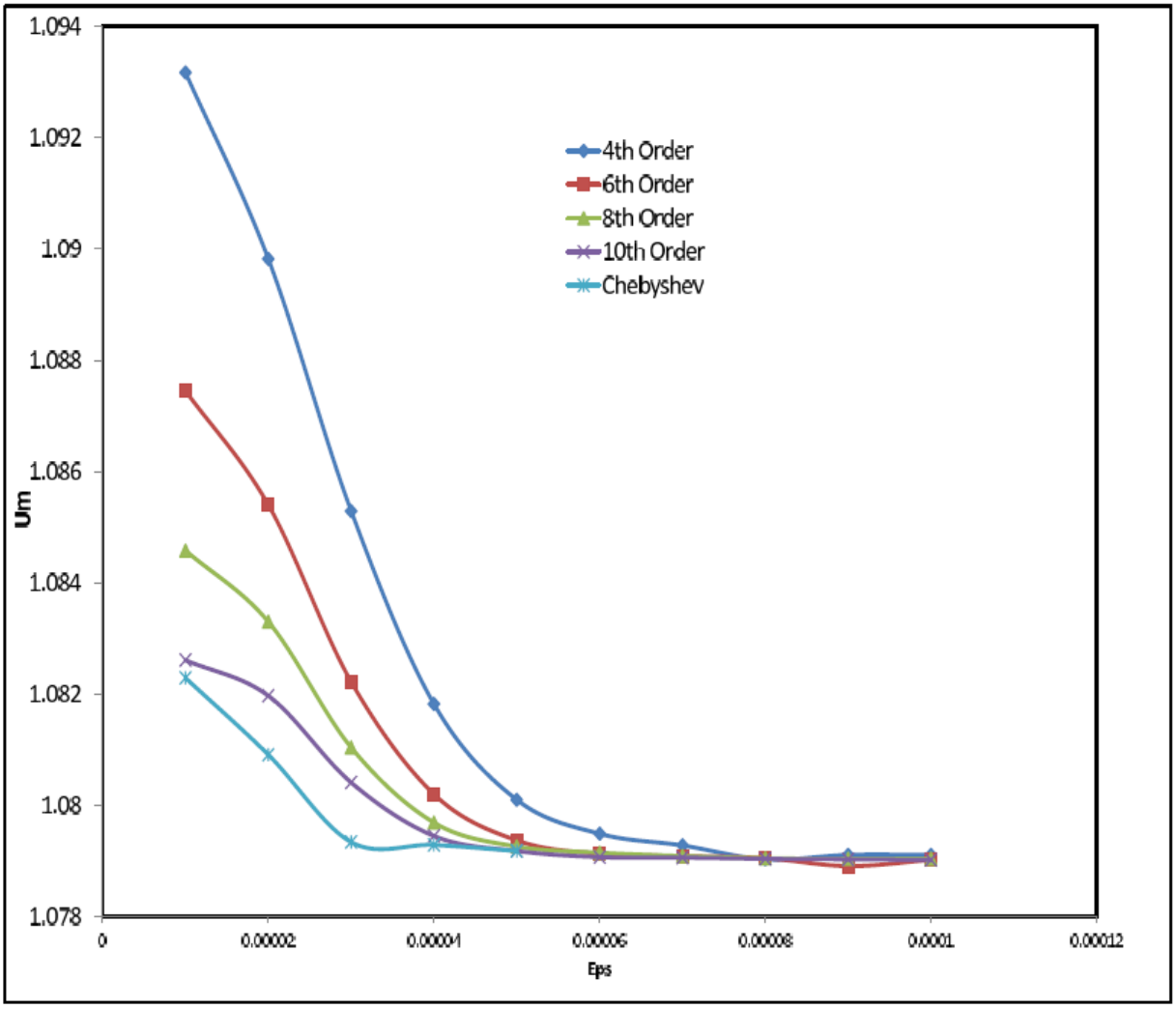

Figure 5.7: The value of the velocity of the middle state versus dispersion coefficient at α=10

5.2 Test 2

Here, another test case is performed to observe the behaviour of the method when initial specific volume is constant and corresponds to the elliptic region. In this case, we consider the following initial left and right states:

$$u_L = 0.1, \qquad \tau_L = 1.2,$$
$$u_R = -0.1, \qquad \tau_R = 1.2$$

Note that the initial specific volume is 1.2, which is in the elliptic region. Since $u_L > 0$ and $u_R < 0$, the above initial condition shows two streams that are colliding. Therefore, the specific volume after the collision should decrease in the intermediate region after the collision and a liquid phase may form.

Therefore, the solution should consist of two shock waves followed by two phase transition boundaries moving outward.

The numerical results of using the Chebyshev pseudospectral method at time $t = 0.5$ using a time-step of 0.0001 with 700 grid points are shown in Figure 18. Viscosity and dispersion coefficients were fixed to the same values of Test 1: $\grave{o} = 3 \times 10^{-5}$ and $\alpha = 10$.

As is observed in Figure 18, the Chebyshev pseudospectral method shows excellent performance in this case and can efficiently capture both shock waves and phase transition boundaries with no significant numerical oscillations.

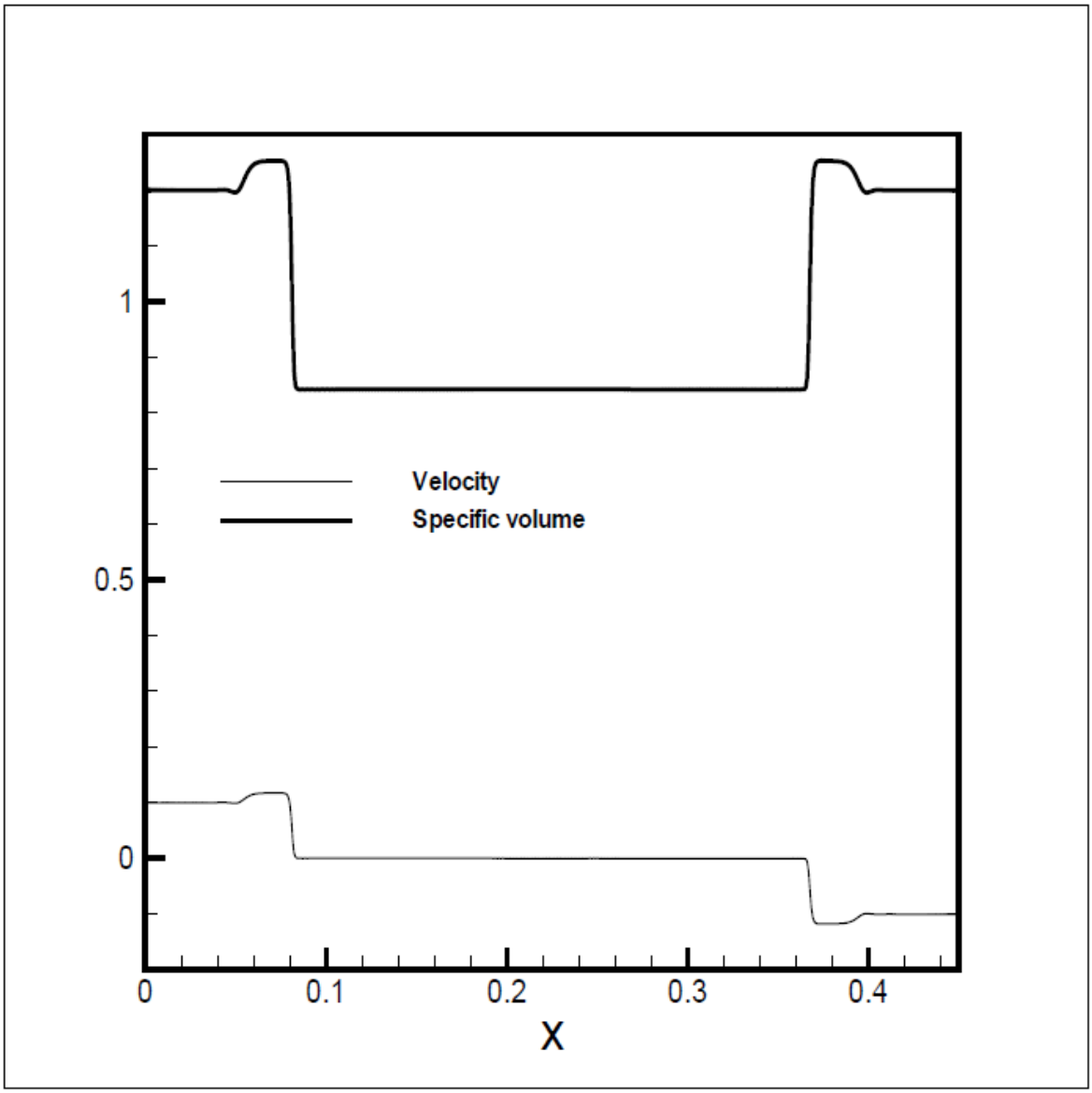

Figure 5.8: Velocity and specific volume using the Chebyshev pseudospectral method at time t=0.5 for Test 2

Finally, it should be mentioned that the proposed scheme is computationally more expensive than the employed finite difference schemes due to the high-order accurate estimation of the derivatives. However, the fact that the proposed scheme is more accurate makes it a better scheme to use as accuracy is very important in numerical simulations. Even if the number of grid

points for the employed finite difference schemes is increased, the numerical oscillations will still be present, which is not the case for the proposed pseudospectral method. Moreover, in practice, the number of grid points cannot always be increased. This is because there are other modules in the numerical model that are also computationally expensive, such as turbulence modeling module. This will make it harder to increase the number of computational grid points and therefore, a scheme which gives better results with a lower number of grid points within a reasonable computational cost is preferable in most practical applications.

Chapter 6: Comparison with Other Schemes

In this chapter we study the effect of temporal integration accuracy by comparing the 4^{th}, 6^{th}, 8^{th}, and 10^{th}-order spatial method using the Crank-Nicolson temporal integration scheme, the 4^{th}-order temporal scheme and the 8^{th}-order temporal scheme. The Central upwind scheme, the Rusanov scheme, and the Fourier pseudospectral method using Fast Fourier Transform (FFT) scheme are also compared with the proposed method.

In the following, we first present the formulation of the above-mentioned schemes and then compare those schemes in terms of accuracy.

6.1 The Central-upwind method

The Central-upwind method is a type of finite volume method. Therefore, as usual, the equations are integrated over control volumes. The divergence theorem is then employed to replace the volume integral with a surface one

$$\frac{d}{dt}\int_{\Omega_c}\vec{U}dx+\int_{\Gamma_c}\vec{F}.\vec{n}a\Gamma_c=0, \tag{6-1}$$

where Γ_c represents the boundary of a control volume, and $\vec{n}$ is its unit outward normal vector.

For the one-dimensional case, the above equation is rewritten either as

$$\frac{d}{dt}\vec{U}_j(t)\Delta x+\left[\vec{F}_{j+1/2}(t)-\vec{F}_{j-1/2}(t)\right]=0 \tag{6-2}$$

or

$$\frac{d}{dt}\vec{U}_j(t) = -\frac{\vec{F}_{j+1/2}(t) - \vec{F}_{j-1/2}(t)}{\Delta x} \tag{6-3}$$

This ODE may be solved using any ODE solver. Here we use the first-order Euler method

$$\frac{\vec{U}_j^{n+1} - \vec{U}_j^{n}}{\Delta t} = -\frac{\vec{F}_{j+1/2}^{n} - \vec{F}_{j-1/2}^{n}}{\Delta x} \tag{6-4}$$

In the Central upwind scheme, the flux is calculated as

$$\vec{F} = \begin{cases} \vec{F}_L & if\,(S_L \geq 0) \\ \vec{F}_R & if\,(S_R \leq 0) \\ \dfrac{S_R\vec{F}_L - S_L\vec{F}_R + S_L S_R(\vec{U}_R - \vec{U}_L)}{S_R - S_L} & otherwise \end{cases} \tag{6-5}$$

For a system with N eigenvalues $a_1,...,a_N$ such that

$$a_1 < a_2 < ... < a_N, \tag{6-6}$$

S_L and S_R are defined as

$$S_L = \min\left(a_1^L, a_1^R, 0\right) \tag{6-7}$$

$$S_R = \max\left(a_N^L, a_N^R, 0\right) \tag{6-8}$$

The solution procedure includes calculation of the flux using (6-5) based on the eigenvalues as explained in (6-6) to (6-8) and then replacing the calculated fluxes in (6-4) to calculate $\vec{U}_j^{n+1}$.

6.2 The Rusanov Scheme

The flux vector $\vec{F}$ in the Godunov-type methods is calculated based on an exact or approximate Riemann solver. Most approximate Riemann solvers are written as

$$\vec{F} = 0.5\left(\vec{F}_R + \vec{F}_L - \Delta\vec{F}^*\right), \tag{6-9}$$

where $\vec{F}_L = \vec{F}\left(\vec{U}_L\right)$ and $\vec{F}_R = \vec{F}\left(\vec{U}_R\right)$ are the left and right flux vectors. The subscripts $\cdot_R$ and $\cdot_L$ represent the evaluations of the right and left sides of the interface, respectively, and $\Delta\vec{F}^*$ is the flux difference. When $\Delta\vec{F}^* = 0$, the scheme is equivalent to a standard centered scheme. Hence, $\Delta\vec{F}^*$ may be considered as an "artificial diffusive flux".

The maximum possible (stable) artificial diffusive flux is employed in the Lax–Friedrich's scheme, which in the 1-D case is written as

$$\Delta\vec{F}^* = \frac{\Delta x}{\Delta t}\Delta\vec{U}, \tag{6-10}$$

where $\Delta\vec{U} = \left(\vec{U}_R - \vec{U}_L\right)$.

A less diffusive approximation for the artificial diffusive flux is that of the Rusanov scheme

$$\Delta\vec{F}^* = -|a_{\max}|(\vec{U}_R - \vec{U}_L), \tag{6-11}$$

where a_{max} is the greatest eigenvalue of the Jacobian matrices corresponding to the left and right flux vectors. The Rusanov scheme is the base of many central schemes, and it provides good results in the case of shock wave problems (see Leveque, 2002 for more details).

The solution procedure is similar to the Central-upwind scheme. First the flux is calculated using sing (6-9)-(6-11) and (6-4) is solved to calculate $\vec{U}_j^{n+1}$.

6.3 The Fourier pseudospectral method

6.3.1 Continuous Fourier series

For a function with period L, a continuous Fourier series can be written as

$$f(x) = a_0 + \sum_{k=1}^{\infty}\left(a_k \cos\left(k\omega_0 x\right) + b_k \sin\left(k\omega_0 x\right)\right) \tag{6-12}$$

Where ω_0 is the wave number given by

$$\omega_0 = 2\pi / L \tag{6-13}$$

And L is the wave length. Using the Euler identity

$$e^{ix} = \cos x + i \sin x \tag{6-14}$$

One obtains

$$\sin x = \frac{e^{ix} - e^{-ix}}{2i}, \tag{6-15}$$

and

$$\cos x = \frac{e^{ix} + e^{-ix}}{2} \tag{6-16}$$

where

$$i = \sqrt{-1} \tag{6-17}$$

Using the above identities, Fourier series can be also expressed in terms of exponential functions:

$$f(x) = \sum_{k=-\infty}^{\infty} \tilde{c}_k e^{ik\omega_0 x} \quad \text{(Inverse Fourier transform)} \tag{6-18}$$

$$\tilde{c}_k = \frac{1}{L} \int_{-L/2}^{L/2} f(x) e^{-ik\omega_0 x} dx \quad \text{(Fourier transform)} \tag{6-19}$$

6.3.2 Discrete Fourier transform

For a periodic function defined on grid points of size Δx

$$f(x) = \sum_{k=-N/2+1}^{N/2} \tilde{c}_k e^{ik\omega_0 x} \quad \text{(Inverse discrete Fourier transform)} \tag{6-20}$$

where

$$\tilde{c}_k = \frac{1}{L} \sum_{j=-N/2+1}^{N/2} c_j \Delta x \qquad c_k = \frac{1}{N} \sum_{j=-N/2+1}^{N/2} c_j \quad \text{(Discrete Fourier transform)}$$

(6-21)

And

$$N = \frac{L}{\Delta x} \tag{6-22}$$

Note that $\sum_{k=-\infty}^{\infty}$ was replaced by $\sum_{k=-N/2+1}^{N/2}$ because the number of data is limited. As the number of data increases, more Fourier modes can be used and the results become more accurate.

There are many algorithms for Fast Fourier Transform. The most popular one was proposed by Cooley and Tukey (1965), and is used in this project.

The solution procedure includes calculation of the flux derivatives based on nodal values of the flux vector as explained in the next section. Once the derivatives are calculated, they are replaced in (3-10) to obtain a semi-discretized equation and then, the semi-discretized system is integrated in time using the fourth order Runge-Kutta method. Note that the derivatives must be calculated at each stage of the Runge-Kutta method using the Fourier pseudospectral method explained in the next section.

6.3.3 Calculation of derivatives using the Fourier expansion

For a set of discrete data, one can find the discrete Fourier transform and then interpolate at any point x using:

$$f(x) = \sum_{k=-N/2+1}^{N/2} \tilde{} \tilde{} \tag{6-23}$$

or

$$f'(x) = \sum_{k=-N/2+1}^{N/2} ik\omega_0 \tilde{f}_k e^{ik\omega_0 x} \tag{6-24}$$

Now, define:

$$\tilde{g}_k \equiv ik\omega_0 \tilde{f}_k \tag{6-25}$$

Thus

$$f'(x) = \sum_{k=-N/2+1}^{N/2} \tilde{g}_k e^{ik\omega_0 x} \tag{6-26}$$

That is, the derivative can be calculated by inverse Fourier transform of $\tilde{g}_k$.

Thus, the algorithm for calculating the first derivative is the following:

1- given f calculate $\tilde{f}$ (using FFT)
2- define $\tilde{g}_k \equiv ik\omega_0 \tilde{f}_k$
3- compute f' from $\tilde{g}_k$ (using IFFT)

The second derivative can be calculated in the same way:

1- given f calculate $\tilde{f}$ (using FFT)
2- define $\tilde{g}_k \equiv -k^2\omega_0^2 \tilde{f}_k$
3- compute f'' from $\tilde{g}_k$ (using IFFT)

A similar approach could be used for higher-order derivatives. The accuracy of these methods is formally spectral. Adding a grid point will add a Fourier mode to the solution. One can calculate all spatial derivatives using FFT instead of using, e.g., finite difference.

6.4 Crank-Nicolson method for temporal integration

For a vector $U(t)$ defined by $U(t) = (u_i(t))_{i=\ldots,-1,0,1,\ldots}$, the semi-discretized scheme may be written as

$$\frac{dU}{dt} = R[U(t)] \tag{6-27}$$

where $R[U(t)]$ is the right-hand side of the van der Waals system. In the Crank-Nicolson method, the above equation is discretized as

$$\frac{U^{`n+1} - U^{`n}}{\Delta t} = \frac{1}{2}\left[R[U(t)]^{n+1} + R[U(t)]^{n} \right. \tag{6-28}$$

6.5 Impact of Temporal Integration Scheme on the Accuracy of the Results

In this test, the impact of time accuracy was examined. This was achieved by comparing the 4^{th}, 6^{th}, 8^{th}, and 10^{th} spatial orders of different temporal schemes (Time Order 4, Time Order 8, and Crank-Nicolson schemes). The Figures 6.1 to 6.4 show the velocity at the middle state versus viscosity coefficient, comparing the space orders, and observing the impact of time order on them. From the graph it can be seen that the impact of time order is not important, as time orders 4 and 8 and Crank-Nicolson schemes appear to be the same. Therefore the temporal accuracy is not significant, and so it can be concluded that time order 4 is enough.

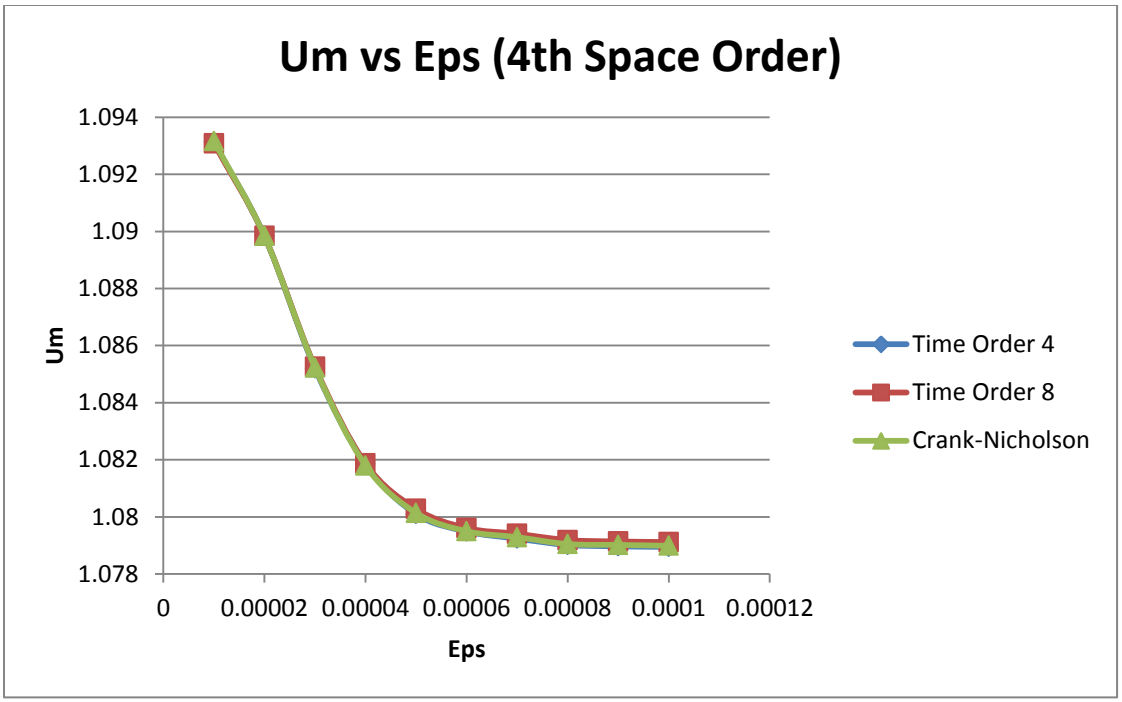

Figure 6.1: Velocity at the middle state versus viscosity coefficient, showing the impact of time order at space order 4

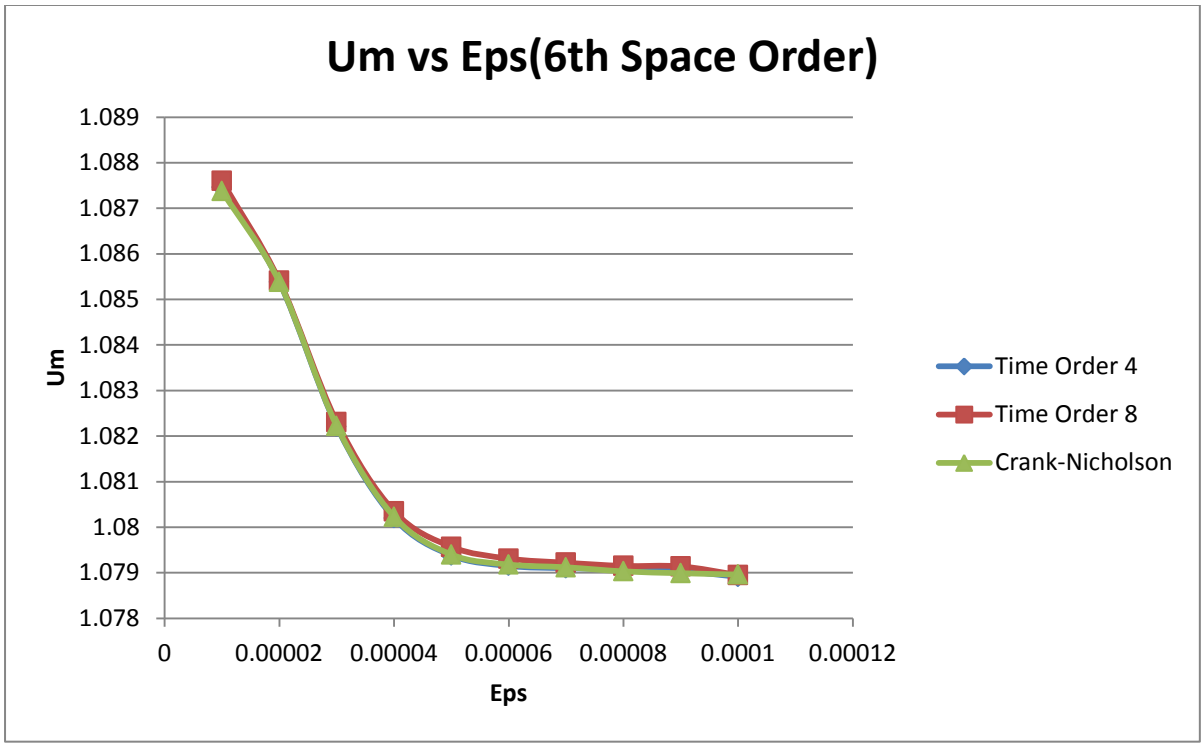

Figure 6.2: Velocity at the middle state versus viscosity coefficient, showing the impact of time order at space order 6

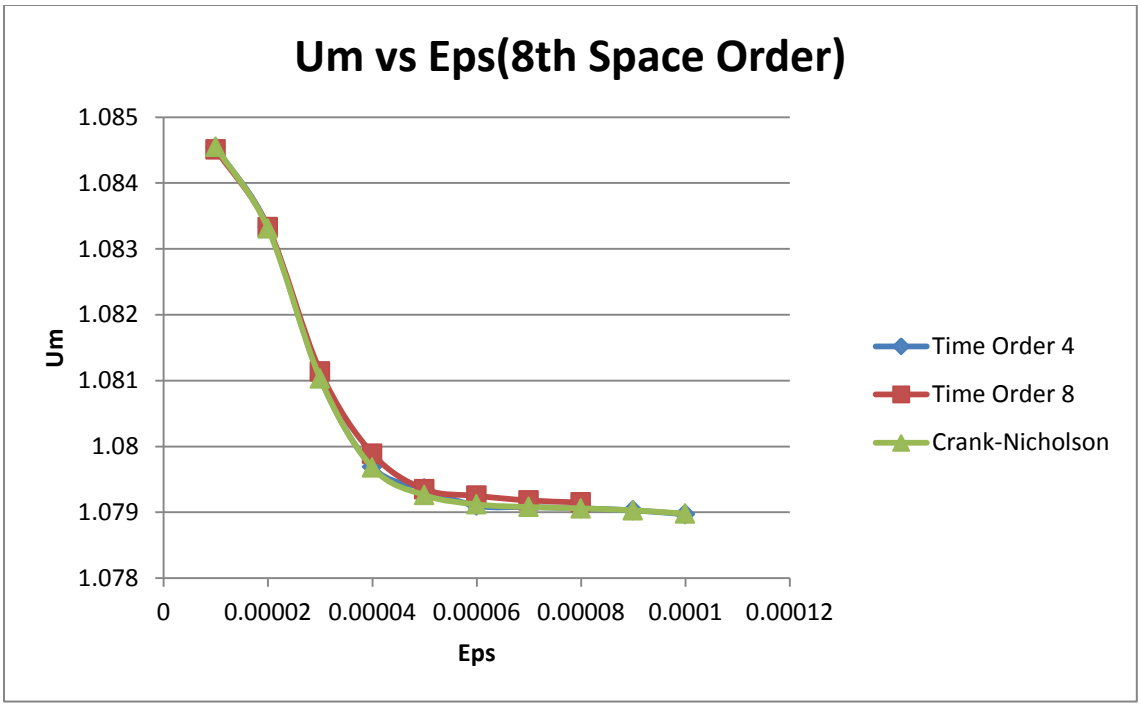

Figure 6.3: Velocity at the middle state versus viscosity coefficient, showing the impact of time order at space order 8

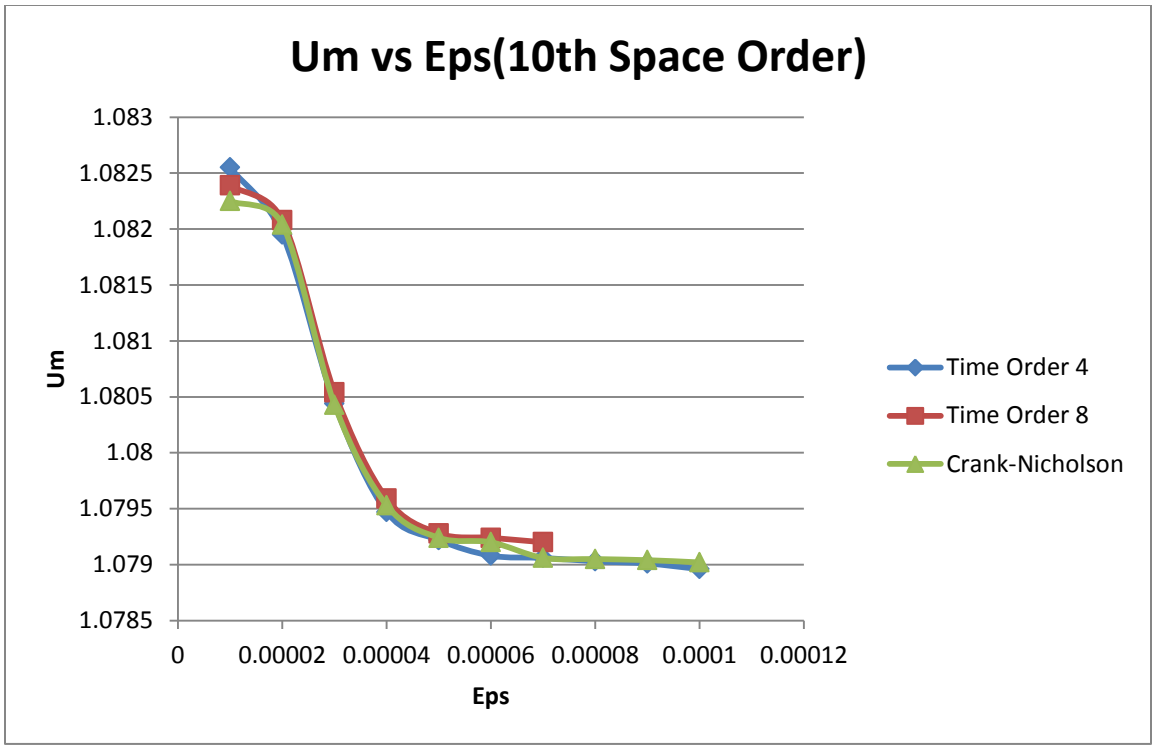

Figure 6.4: Velocity at the middle state versus viscosity coefficient, showing the impact of time order at space order 10

6.6 Comparison with the Central Upwind Scheme

It is now clear that time order 4 is enough and we do not need to increase the order of accuracy of the temporal integration scheme, as the impact of time order is not significant. In this section, the Central upwind scheme is compared with the 4^{th}, 6^{th}, 8^{th}, 10^{th} –order finite difference methods and the Chebyshev pseudospectral scheme. Figure 6.5 shows the value of the velocity at the middle state versus the viscosity coefficient for the various space orders at time order 4, compared with the Chebyshev and Central upwind schemes. It can be seen that the Central upwind scheme is not as accurate as the Chebyshev pseudospectral method, and is actually even less accurate than the fourth-order scheme.

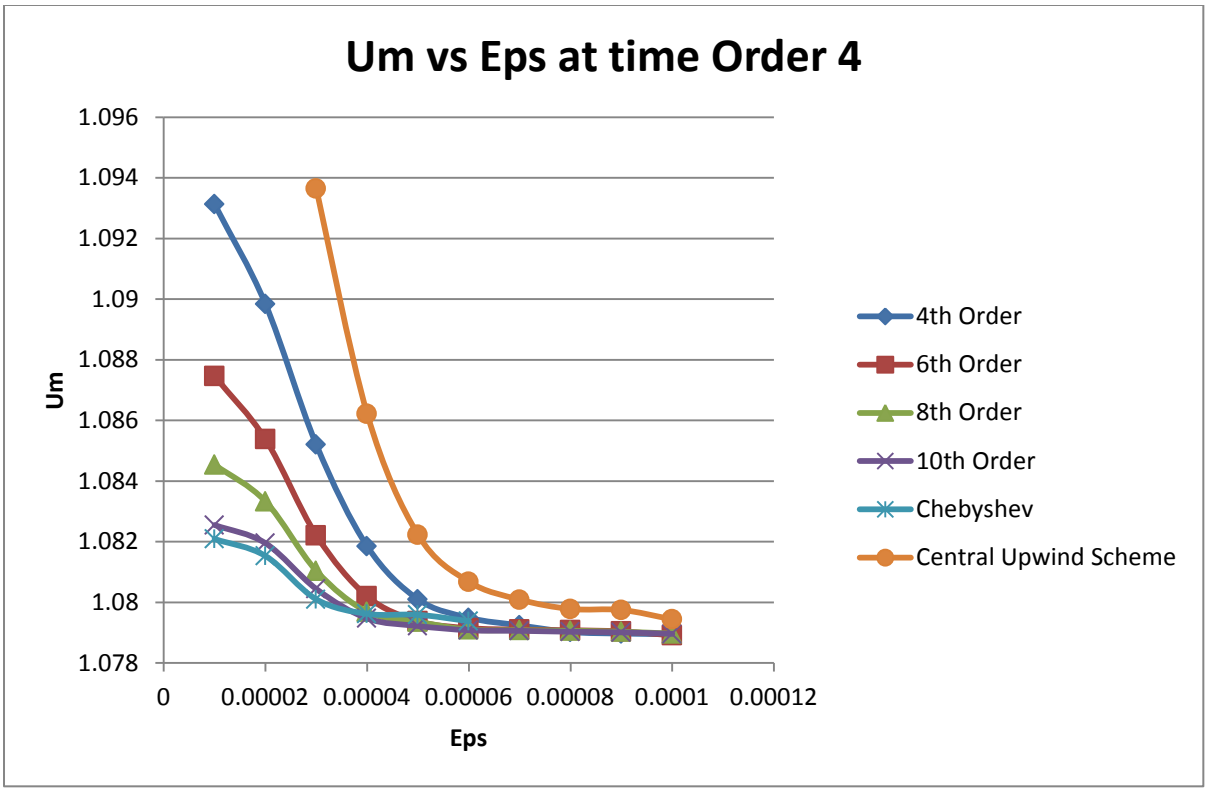

Figure 6.5: Velocity at the middle state versus viscosity coefficient, comparing the Chebyshev scheme with the Central upwind scheme

6.7 Comparison with the Fourier Pseudospectral Scheme

In this test, the Fourier pseudospectral method with Fast Fourier Transform (FFT) scheme is compared to the Chebyshev pseudospectral method, and the results are shown in Figure 6.6. As can be seen from Figure 24, for large ε values the results of the Fourier pseudospectral method are only as accurate as the fourth-order finite difference scheme, and for small ε values the method shows a non-monotonic behaviour which is not desirable. Therefore, noting that the computational cost of this method is much higher than the fourth-order finite difference scheme, it could be concluded that the Fourier pseudospectral method is not a suitable scheme for the van der Waals system.

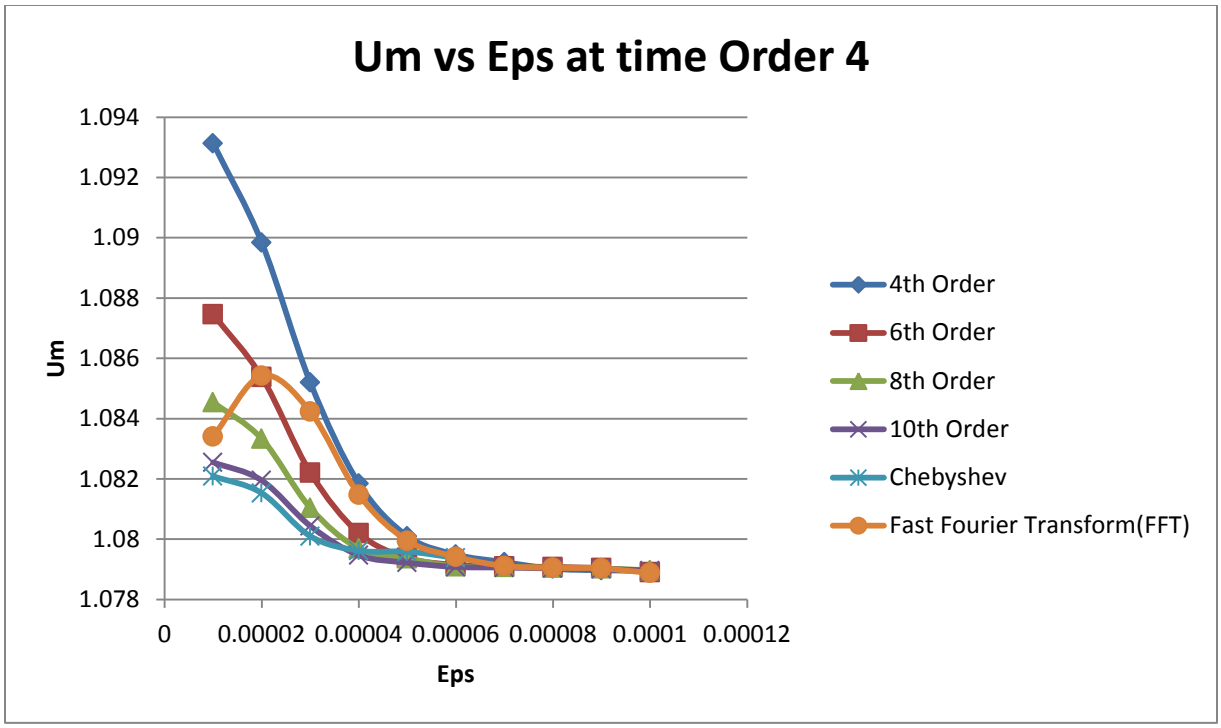

Figure 6.6: Velocity at the middle state versus viscosity coefficient, comparing Chebyshev scheme with Fourier pseudospectral scheme

6.8 Comparison with the Rusanov Scheme

Finally, here the Rusanov method is compared with the Central upwind method for modelling van der Waals fluids, and the results are shown in Figure 6.7. As can be seen in Figure 6.7, the two methods show almost identical results. Therefore, based on the poor performance of the Central upwind scheme as seen in Figure 6.5, we can conclude that the Rusanov method is also not as accurate as the proposed Chebyshev pseudospectral method.

In summary, in this chapter, three further spatial discretization schemes, including the Fourier pseudospectral method, the Central-Upwind scheme, and the Rusanov method were compared with the proposed Chebyshev pseudospectral method, and it was found that the performance of the Chebyshev pseudospectral method is better than all other considered schemes. Moreover, two

other time discretization schemes, including the Crank-Nicolson method and the eight-order Runge-Kutta temporal integration schemes, were also compared with the employed fourth-order Runge-Kutta method for time integration, and again it was found that the results are rather insensitive to the order of temporal integration schemes, and given the moderate computational cost of the fourth-order Runge-Kutta method, it can be recommended for temporal integration.

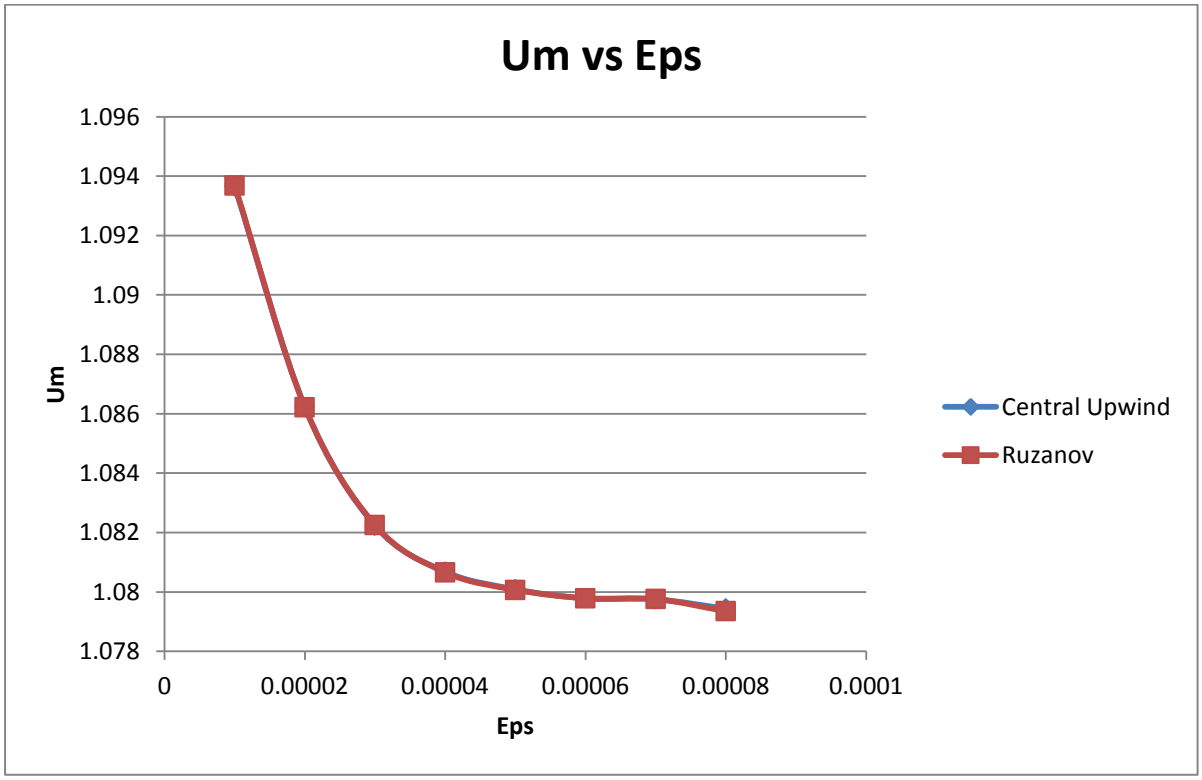

Figure 6.7: Velocity at the middle state versus viscosity coefficient, comparing Rusanov scheme with the Central upwind scheme

Chapter 7: Conclusion

Liquid-vapour flows constitute an important part of the problems in fluid mechanics, and their correct simulation is important both for modelling of problems with phase changes and for development of turbulence closures. As explained in Chapter 2, in certain cases, the intermolecular forces are not negligible; the ideal gas equation of the state is not valid for such cases, and small-scale effects such as intermolecular forces become important. Therefore, the van der Waals equation of state should be used for correct modelling of these flows. Such flows may be observed in some applications such as certain industrial refrigerators and refrigerated nuclear reactors.

When standard finite-difference space discretization schemes are used for the corresponding equations, usually numerical errors appear. When the order of accuracy of the semi-discrete scheme is increased, these numerical errors are still present in the equations. Such dispersive numerical oscillations can affect the accuracy of the numerical solution. Another problem arises from the elliptic part of the solution domain, which is very sensitive to small perturbations.

Numerical oscillations that are generated due to the employed numerical method are generally undesirable because they may be reflected back into the domain from the boundaries and interact and be even amplified. In such cases, the numerical simulation becomes inaccurate due the presence of these numerical oscillations which make it difficult to simulate physical oscillations that are also present in such problems, e.g. due to capillarity effects.

Considering a Riemann problem with left- and right-hand states in the hyperbolic regions of the solution, the standard entropy criterion for purely hyperbolic systems cannot be used to detect

unphysical solutions for these flows. This is due to the possible presence of non-classical shock waves, namely phase boundaries, which violate the standard entropy criterion (see e.g., LeFloch, 2002) and the so-called kinetic relation, is usually used to uniquely specify the solution. Numerical modelling of these flows is a challenging problem. In particular, numerical methods may lead to inaccurate kinetic functions (LeFloch and Mohammadian, 2008) for these flows, as is also shown in LeFloch (2002), using analysis of the modified equation. The present project focused on the quest for numerical methods able to deal with the mixed nature of the governing system of differential equations of these fluids. From the numerical point of view, the solution of this class of Riemann problems can be approached by augmenting the momentum equation with a viscous term as well as a dispersive term representing capillarity. However, the calculated kinetic function is sensitive to the ratio of numerical diffusion to numerical dispersion.

From a physical point of view, the non-classical shock wave represents phase separation. In many problems in fluid mechanics, only a low level of numerical diffusion is acceptable, such as in direct numerical simulations of turbulent flows. For such cases, spectral methods are usually preferred because of their high level of accuracy (see e.g., Mohammadian & Charron, 2011). Two main groups of spectral methods which have been widely used in fluid mechanics are the Fourier and Chebyshev methods. In Fourier spectral methods, the basis functions are trigonometric functions, and therefore they are mainly used for periodic boundaries. On the other hand, in Chebyshev spectral methods, polynomials are used as basis functions and are more popular for non-periodic boundaries. Generally in such methods, by adding a grid point the numerical error is reduced for two reasons, the reduction of grid size and the increase in the order of accuracy, because the degree of approximating polynomials increases. The numerical kinetic function associated with various high-order schemes for van der Waals fluids was calculated in

LeFloch and Mohammadian (2008), and they showed that the accuracy of the kinetic function increases by increasing the order of accuracy of spatial discretization schemes. Therefore, due to their high order of accuracy and in accordance with the conclusion of LeFloch and Mohammadian (2008), the Chebyshev spectral method could be a good numerical method for modelling non-classical shock waves and phase transition boundaries.

In most nonlinear problems, direct application of spectral methods is not possible, and so pseudospectral methods are used instead. In such methods, the derivatives are calculated in the space of basis functions, but the nonlinear terms are calculated in the physical space by transforming the calculated derivatives back from the space of basis functions to the physical space.

The main objective of this project was to find an appropriate numerical method which leads to a lower level of numerical oscillations and higher accuracy. Several commonly used numerical methods were examined and their performance in simulating shock waves in van der Waals flows was studied. The selected schemes include the Chebyshev pseudospectral method, the Rusanov scheme, the Central-upwind method, Fourier pseudospectral scheme and the Crank-Nicolson method.

An experimental methodology was employed in this project. Our criteria to compare various numerical methods were the presence and level of numerical oscillations. The high order finite difference schemes studied in LeFloch and Mohammadian (2008) were considered as reference solutions. In in LeFloch and Mohammadian (2008), it was concluded that as the order of the accuracy of the finite difference methods increases, their results become more accurate and their kinetic function becomes closer to the analytical kinetic function. Therefore, in this study, the

limiting solution of high order finite difference schemes was considered as the reference solution. We looked for a numerical method that leads to the lowest lower level of numerical oscillations and also leads to a solution closer to the limiting solution obtained by high order finite difference methods. A summary of the results is given in section 7.1.

As the result of the numerical studies, the use of the Chebyshev pseudospectral method was proposed for a class of van der Waals flows with mixed hyperbolic-elliptic behaviour for which eigenvalues of the system are not always real. Between certain values of the specific volume the eigenvalues become imaginary, and therefore the governing system of PDEs become elliptic. Standard numerical methods for simulation of hyperbolic systems such as upwind finite volume methods, which are based on wave propagation algorithms, cannot be used for these equations due to the fact that in the hyperbolic regime the system has no characteristics. Such systems allow for under-compressive non-classical shock waves whose kinetic functions may be non-monotonic and non-single-valued. Such non-classical shock waves are the phase transition boundaries.

7.1. Summary of results

A summary of the conclusions obtained in this thesis is given below:

1. The numerical results of the Chebyshev pseudospectral method were compared with the high-order finite difference schemes (up to tenth-order) illustrated in LeFloch and Mohammadian (2008), which showed that the proposed method leads to better results.
2. Sensitivity analyses were also performed with respect to diffusive and dispersive coefficients, and the appropriate values for those parameters were obtained such that the shock waves and phase transition boundaries are appropriately modelled. The sensitivity

of various schemes with respect to those parameters was also examined.

3. Numerical kinetic functions were obtained for various schemes that could be used to rule out physically incorrect phase transition boundaries.
4. The Chebyshev pseudospectral method performs better than all other employed finite difference and finite volume schemes, with a lower level of numerical diffusion and oscillations. The numerical methods that were included in the comparisons included the Central upwind scheme, the Rusanov method, and the Fourier pseudospectral scheme.
5. The Chebyshev pseudospectral method does not lead to fast short-wave noise packages which move to the right- and left-hand sides ahead of the rarefaction and shock waves, which is typically observed in finite difference schemes. In addition, it performs well in all complex regimes, such as mixed hyperbolic-elliptic ones.
6. Temporal accuracy of the employed numerical method is less important than the spatial accuracy. The performance of the fourth- and eighth-order schemes is similar. Moreover, the Crank-Nicolson scheme is also similar to those two schemes.
7. The Rusanov and Central upwind schemes lead to similar results which are not accurate. They induce a high level of dissipation in the numerical method.
8. Contrary to expectations, the Fourier pseudospectral method is not accurate for the van der Waals fluids. Although the accuracy of this method is formally spectral, it is not as accurate as the Chebyshev pseudospectral method.
9. The Chebyshev pseudospectral method leads to accurate results when the initial value of specific volume corresponds to the elliptic region.

7.2 Future work

In this work, the variables considered are specific volume (τ) and velocity (u). In future studies, the impact of the change of variables proposed by Cockburn, B., Gau, H. (1996), could be examined. This approach has also been employed in Pecenko et al. (2010) and promising results have been obtained. Also in this thesis, the Chebyshev pseudospectral method was compared to the 2^{nd}- 10^{th} finite difference schemes, the Central upwind scheme, the Rusanov scheme and the Fourier pseudospectral method. Not all popular methods for modelling van der Waals fluid were considered. For example, fully discrete schemes such as, the Lax-Friedrichs, Beam- Warming and Lax-Wendroff schemes could be also considered and compared with the Chebyshev pseudospectral method for the numerical modelling of liquid-vapour flows.

References

Baltensperger, R., Berrut, J.P., (1999). The errors in calculating the pseudospectral differentiation matrices for Chebyshev-Gauss-Lobatto points. *Journal of Computers & Mathematics with Applications, 37, 41-48.*

Bayliss, A., Class, A., Matkowsky, B. J., (1994). Round-off errors in computing derivatives using the Chebyshev differentiation matrix, *Journal of Computational Physics*, 116, 380-383.

Canuto C., Hussaini M., Quarteroni A., Zang T., (2006). Spectral methods, *fundamentals in single domains*, Springer, Berlin.

Cockburn, B., Gau, H., (1996). A model numerical scheme for the propagation of phase transitions in solids. *SIAM Journal of Scientific Computing,* 17, 1092.

Holms, H. ,Clamond, D., Langtangen, H. P., (2008). A pseudospectral Fourier method for a 1D incompressible two-fluid model, *International Journal for Numerical Methods in Fluids*, 58, 6, 639-658.

Kondaraju S., Xu X., Lee J.-S., (2010). Direct numerical simulation of preferential particle concentration in decaying turbulence under the influence of magnetic field, *International Journal for Numerical Methods in Fluids*, 63, 1233–1240.

Kreiss, H.O., Oliger, J., (1972) Comparison of accurate methods for the integration of hyperbolic equations, Tellus, 24, 299-215.

LeFloch, P.G., (2002). Hyperbolic systems of conservation laws: the theory of classical and non-classical shock waves, *Lectures in Mathematics*, ETH Zürich, *Birkäuser*.

LeFloch, P. G., Mohammadian, M., (2008).Why many theories of shock waves are necessary: kinetic functions, equivalent equations, and fourth-order models. *Journal of Computational Physics*, 227(8), 4162-4189.

Le Roux, D. Y., Rostand, V, Pouliot, B., (2008). Analysis of numerically-induced oscillations in 2D finite-element shallow water models part I: inertia gravity waves. *SIAM Journal on Scientific Computing*, 29,331-360.

Le Roux, D. Y., Pouliot, B., (2008). Analysis of numerically-induced oscillations in two-dimensional finite-element shallow water models part II: free planetary waves. *SIAM Journal on Scientific Computing*; 30,1971-1991.

LeVeque, R.., (2002). Finite Volume Methods for Hyperbolic Problems, Cambridge University Press.

Li, B.W., Zhao, Y.R., Yu, Y., Qian, Z.D., (2010) Three-dimensional transient Navier-Stokes solvers in cylindrical coordinate system based on a spectral collocation method using explicit treatment of the pressure, *International Journal for Numerical Methods in Fluids*, In press.

Majda, A., Mohammadian, M., Xing, Y., (2008). Vertically Sheared Horizontal Flows with Mass Sources: A Canonical Balanced Model, *Geophysical and Astrophysical Fluid Dynamics*, 102, 6, 543-591.

Makinde O. D., (2009). On the Chebyshev collocation spectral approach to stability of fluid flow in a porous medium, *International Journal for Numerical Methods in Fluids*, 59, 7, 791-799.

Mohammadian, A., Charron, M., (2011). Analytical and Chebyshev Pseudospectral Numerical Solutions for a Class of Axisymmetric Horizontal Flows Dominated by Mass or Heat Sources, *International Journal for Numerical Methods in Fluids.*

Mohammadian, M., Marshall, J., (2010). A Vortex in Cell Model for the Quasi- Geostrophic Dynamics, In press in Ocean Modeling.

Mohammadian, M., Le Roux, D., (2008). Fourier Analysis of a Class of Upwind Schemes in Shallow Water Systems for Gravity and Rossby waves, *International Journal for Numerical Methods in Fluids*, 57, 4, 389-416.

Mohammadian, M., Le Roux, D., (2006). Simulation of Shallow Flows over Variable Topography Using Unstructured Grid, *International Journal for Numerical Methods in Fluids*, 52, 5, 473-498.

Mohammadian, A., Le Roux, D., Tajrishi, M., Mazaheri, K., (2005). A Mass Conservative Scheme for Simulating Shallow Flows over Variable Topography Using Unstructured Grid, *Advances in Water Resources*, 28, 523-537.

Noelle, S. , Xing, Y., Shu, C.W., (2007). High-order well-balanced finite volume WENO schemes for shallow water equation with moving water, *Journal of Computational Physics*, 226, 10, 29-58.

Orszag, S. A., (1972). Comparison of pseudospectral and spectral approximations, *Studies in Applied Mathematics*, 51, 253-259.

Orszag, S. A., Patterson, G. S., (1972). Numerical simulation of three dimensional homogeneous isotropic turbulence, *Physics Review Letters*, 28, 76-79.

Pecenko, A., Kuerten, J., Van der Geld, C., (2010). A diffuse-interface approach to two-phase isothermal flow of a Van der Waals fluid near the critical point. *International Journal of Multiphase Flow*, 36, 558-569. 23.

Peyret, R., (2002). Spectral methods for incompressible viscous flow, Springer, Berlin.

Sengupta, K., Jacobs, G. B., Mashayek, F., (2009). Large-eddy simulation of compressible flows using a spectral multidomain method, *International Journal for Numerical Methods in Fluids*, 61, 3, 311-340.

Slemrod, M., (1983). Admissibility criteria for propagating phase boundaries in a van der Waals fluid, *Arch. Ration. Mech.* Anal, 8(1) 301-315.

Tenaud, C., Garnier, E., Sagaut, P., (2000). Evaluation of some high-order shock capturing schemes for direct numerical simulation of unsteady two-dimensional free flows, *International Journal for Numerical Methods in Fluids*, 33, 2, 249-278.

Tsitouras, C., (2001). Optimized explicit Runge-Kutta pair of order 9. *Applied Numerical Mathematics*, 38,123--134.

Tsitouras, C., Papakostas, S.N., (1999). Cheap error estimation for Runge-Kutta methods. *SIAM Journal of Scientific Computing*, 20, 2067--2088.

Trefethen, L., (2000). Spectral Methods in MATLAB. *SIAM*, Philadelphia

Xie, M. L., Lin J. Z., (2009) An efficient numerical solution for linear stability of circular jet: A combination of Petrov-Galerkin spectral method and exponential coordinate transformation based on Fornberg's treatment, *International Journal for Numerical Methods in Fluids,* 61, 7, 780-795.

Xing, Y., Shu, C.W., (2006). High order well-balanced finite volume WENO schemes and discontinuous Galerkin methods for a class of hyperbolic systems with source terms, *Journal of Computational Physics*, 214, 567-598.